Development of relativistic electronic structure theory for solvated molecules based on the integral equation theory of molecular liquid

金丸, 恒大

出版情報：Kyushu University, 2022, 博士（理学）, 課程博士
バージョン：
権利関係：

Development of relativistic electronic structure theory for solvated molecules based on the integral equation theory of molecular liquid

Doctoral Thesis

Kodai Kanemaru

Graduate school of science

2023

Contents

Chapter 1.

General introduction

Molecules containing heavy elements are utilized in various fields, such as catalysis, anti-cancer agents, material for luminescence, and nuclear fuels. Nowadays, the importance of relativistic effects on these molecules is well recognized. Relativistic effects can be classified into spin-free and spin-dependent effects. Spin-free effects are also called scalar relativistic effects and mainly contribute to orbital contraction and expansion. An example of where these effects are essential role is in the trend of bond lengths in coinage element monohydrides. On the other hand, spin-dependent effects, which include spin-orbital coupling, are essential role in mainly molecular properties. For example, the absorption in the near-infrared region originating from the spin-forbidden transition of osmium complexes cannot be qualitatively reproduced without this effect. Therefore, in today's quantum chemical calculations, relativistic effects must be treated appropriately.

Relativistic effects have added a new dimension to the concept of theoretical model chemistries originally was proposed by People and are introduced through the choice for Hamiltonian. These relativistic effects are most fundamentally described by the Dirac equation, which is the basic equation of relativistic quantum mechanics:[1]

$$\begin{bmatrix} \hat{V} & 0 & \hat{p}_z & \hat{p}_x - i\hat{p}_y \\ 0 & \hat{V} & \hat{p}_x + i\hat{p}_y & -\hat{p}_z \\ \hat{p}_z & \hat{p}_x - i\hat{p}_y & \hat{V} - 2c^2 & 0 \\ \hat{p}_x + i\hat{p}_y & -\hat{p}_z & 0 & \hat{V} - 2c^2 \end{bmatrix} \begin{bmatrix} \Psi_\alpha^{\mathrm{L}} \\ \Psi_\beta^{\mathrm{L}} \\ \Psi_\alpha^{\mathrm{S}} \\ \Psi_\beta^{\mathrm{S}} \end{bmatrix} = E \begin{bmatrix} \Psi_\alpha^{\mathrm{L}} \\ \Psi_\beta^{\mathrm{L}} \\ \Psi_\alpha^{\mathrm{S}} \\ \Psi_\beta^{\mathrm{S}} \end{bmatrix}. \qquad (1.1)$$

This equation gives a wavefunction with four components as its solution. Among several relativistic methods, the method that treats all four components explicitly is called “four-component method”. Alternative methods treating relativistic effects are so-called “two-component method”. The two-component method is also widely used in quantum chemical calculations due to less computational demanding compare with four-component method. The four-component spinor in Eq(1.1) can be classified into large and small components. The large component is a large contribution to an electronic solution of Eq(1.1). On the other hand, the small component is a small contribution to an electronic solution but large contribution to a positronic solution. The two-component method uses only the degree of freedom of electrons decoupled from that of positrons. The two-component spinors used in this method are

transformed spinors that are decoupled from the degrees of freedom of positrons and thus are not identical to any parts of the original four components. Decoupling degree of freedom is accomplished by block diagonalization (approximately or exactly) of Dirac equation using transformation:

$$\mathbf{U}\mathbf{H}_{\mathrm{D}}\mathbf{U}^{\dagger} = \begin{bmatrix} \mathbf{H}^{+} & 0 \\ 0 & \mathbf{H}^{-} \end{bmatrix}. \qquad (1.2)$$

A unitary transformation even satisfy exactly Eq(1.2) cannot be determined uniquely. There are many versions of two-component depending on the transformation matrix **U**. In two-component method, an inherit error which is called “picture-change error” (PCE) exists. PCE is caused by inconsistency of basis, and thus an artificial error. PCE affect molecular electron density especially near nuclear region. Nuclear shielding tensor is representative of a property for which the electron density near nucleus region is important. To calculate such a molecular property in solution phase accurately, picture-change correction can be regarded as one of key issues.

To date, various electronic structure methods used in nonrelativistic quantum chemistry have been extended to relativistic four- and two-component Hamiltonian. For accurate description in solution phase, solvent effects must be treated. In modern quantum chemical calculation, development of method including relativistic effects, electron correlation, and solvent effects simultaneous is desired for accurately description of chemical phenomena of heavy element containing molecules. Thus, development of a method that can handle both relativistic and solvent effects simultaneously can be regarded as an important issue in computational chemistry. In this thesis, two methods are proposed to develop a method that can handle both relativistic and solvent effects simultaneously: a hybrid method of four-component relativistic method and integral equation theory of molecular liquid and two-component method based on quasi-degenerate perturbation theory. In chapter 2, a hybrid method of four-component Dirac-Hartree-Fock and reference interaction site model self-consistent field (DHF/RISM-SCF) is presented as treating relativistic and solvent effects simultaneous. In chapter 3, application of DHF/RISM-SCF to chemical reaction is presented. In chapter 4, a two-component method based on QDPT was formulated.

Chapter 2.

Solvent effects in four-component relativistic electronic structure theory based on the reference interaction-site model

2.1 Introduction

The relativistic molecular orbital theory is now one of the essential pieces in quantum chemical theory. Currently, it is well recognized that the relativistic effects have an important role in the electronic structure of molecules containing heavy elements. In particular, the scalar and spin–orbit effects, which are classes of relativistic effects, affect the geometries, properties, and reactions of molecules through their effects on the shape of molecular orbitals and splitting of energy levels. Such relativistic effects are most naturally taken into account via the Dirac equation, which is the basic equation of relativistic quantum mechanics.[1] The Dirac equation gives four-component spinors as solutions describing the electrons and their anti-particles, the positrons. The methods based on the Dirac equation are called four-component methods, and are now widely used in quantum chemistry, along with the two-component methods. Nowadays, the relativistic Hartree–Fock (HF)[2–5], the density functional theory (DFT)[6,7], Møller–Preset perturbation[8–10], configuration interaction (CI)[11,12], and coupled-cluster (CC)[13] methods have been developed and standardly used. In addition to the HF, DFT, and HF-based single reference methods, multiconfiguration methods, such as the multiconfiguration self-consistent field (MCSCF) method[14,15], multireference (MR) CI[16], MR perturbation[17–19], and MR CC[20] methods, were developed and are being used. Recently, the four-component full CI Monte Carlo[21] and density matrix renormalization group[22] were formulated.

When considering chemical reactions in solution of molecules containing heavy atoms, solvent effects must be considered simultaneously with relativistic effects. The methods for incorporating the solvent effects on the four-component relativistic methods have been fairly limited to date, and a methods combined with the polarizable continuum model (PCM) has recently been proposed by Di Remigio et al.[23] They formulated a four-component relativistic self-consistent field (SCF) theory for a molecular solute described with the PCM for solvation. In their study, the four-component Dirac–Hartree–Fock and Kohn–Sham DFT methods were

combined with the integral equation formalism (IEF) PCM[24] to successfully determine the electronic structure of the solute and the continuum model of the solvent in a self-consistent manner. After being proposed, this method has been applied to the calculations of electron paramagnetic resonance and nuclear magnetic resonance (NMR) parameters, etc.[25] The four-component relativistic polarizable embedding was also presented by Hedegård et al. in 2017.[26]

In the present article, we present the four-component Dirac–Hartree–Fock reference interaction-site model self-consistent field (DHF/RISM-SCF) method, which combines the relativistic four-component method with the reference interaction-site model (RISM), and its geometrical derivative have been formulated and implemented. RISM[27,28] is a statistical-mechanical integral equation theory for molecular liquids, which is derived from the functional derivative of the grand potential for solute–solvent molecular pair interactions with respect to the density function. Features different from the PCM are that the RISM theory can account for intermolecular interactions such as hydrogen bond and that it can provide a solvation structure around the solute molecule. Furthermore, an analytical solvation free energy expression is known and can be evaluated based on a first-principles approach. These advantages have led to its use in the analysis of various chemical processes in solution.[28] A hybrid method of quantum chemical electronic structure and the RISM theories, called RISM-SCF method, was proposed by Ten-no et al., in 1993.[29,30] The coupled equations of the Hartree–Fock and RISM equations derived by them are solved self-consistently, and the electronic wave function of the solute molecule and the solvent distribution can be determined simultaneously. Following their study, the combination of the theories has been variously extended both in the electronic structure and integral equation theories.[31,32] Therefore, the RISM theory is also effective in introducing solvent effects into the relativistic electronic structure theory. The DHF/RISM-SCF method presented here, enables the simultaneous description of the detailed solute electronic structure based on the relativistic electronic structure theory and the solvation structure based on molecular theory.

This chapter is structured as follows. The DHF/RISM-SCF method based on variational formalism as well as its analytical energy gradient method is presented in Section 2.2; the computational details are given in Section 2.3; the applications to several systems (the iodine ion I^-, methyl iodide CH_3I, and hydrogen chalcogenides H_2X (O–Po) are discussed in Section 2.4; and conclusions are drawn in Section 2.5.

2.2 Theory

The RISM-SCF method is formulated as a variational problem for free energy, which was initially proposed by Sato et al.[31] for an MCSCF wave function. Here, we consider a system in which a quantum mechanical solute molecule is immersed in a solvent composed of classical molecules at infinite dilution. In this formulation, the basic equations are derived from the stationary conditions for the Helmholtz energy Lagrangian:

$$L\left(\mathbf{C}, \boldsymbol{\zeta}^{\mathrm{U}}, c, h, t\right) = E^{\mathrm{U}}(\mathbf{C}) + \Delta\mu(\mathbf{C}, c, h, t) + \boldsymbol{\zeta}^{\mathrm{U}} \cdot \boldsymbol{e}^{\mathrm{U}}(\mathbf{C}). \tag{2.1}$$

The first term of the right-hand side in Eq. (1) represents the electronic energy of the solute molecule and $\mathbf{C}$ is the set of the variational parameters in the wave function. The second term represents the excess chemical potential of solvation, and c, h, and t are the direct, total, and indirect correlation functions describing the solvent structure around the solute molecule, respectively. The third term corresponds to constrains on the parameters ($\mathbf{C}$) in the solute wave function; i.e., the orthonormality of orbitals and/or the normalization of the wave function. The symbols $\boldsymbol{e}^{\mathrm{U}}$ and $\boldsymbol{\zeta}^{\mathrm{U}}$ are the sets of constrains and multipliers, respectively.

The solute energy $E^{\mathrm{U}}(\mathbf{C})$ depends on the electronic structure method used, which will be discussed later. The form of the excess chemical potential $\Delta\mu$ depends on the closure employed. Several closures have been proposed and used, and each has its own advantages. Here, we use hypernetted chain (HNC) closures and its n[th] order partial series expansion. Then, the excess chemical potential is rewritten in Eqs. (2.2) and (2.3), as follows:

$$\begin{aligned}
\Delta\mu(\mathbf{C}, c, h) &= \sum_{\alpha s}\left(\Delta\mu_{\alpha s}^{\mathrm{HNC}} - \beta^{-1} n_s \int \mathrm{d}\mathbf{r}\, \Theta\big(h_{\alpha s}(r)\big) \frac{\big(t_{\alpha s}(r) - \beta u_{\alpha s}(C, \zeta, r)\big)^{n+1}}{(n+1)!}\right) \\
&= \beta^{-1} \sum_{\alpha s} n_s \int \mathrm{d}\mathbf{r}\, [\big(1 - \Theta\big(t_{\alpha s}(r) - \beta u_{\alpha s}(r)\big)\big)\big(\exp\big(t_{\alpha s}(r) - \beta u_{\alpha s}(r)\big)\big) \\
&\quad + \Theta\big(t_{\alpha s}(r, \lambda) - \beta\lambda u_{\alpha s}(r)\big)\left(\sum_{i=0}^{n} \frac{1}{i!}\big(t_{\alpha s}(r) - \beta u_{\alpha s}(r)\big)^{i}\right) \\
&\quad - t_{\alpha s}(r) - h_{\alpha s}(r) t_{\alpha s}(r) + \frac{1}{2} h_{\alpha s}^2(r)] \\
&\quad - \frac{\beta^{-1}}{(2\pi)^3} \int \mathrm{d}\mathbf{k} \left[\frac{1}{2} \sum_{\alpha, s, \gamma, t} \hat{c}_{\alpha s}(k) \hat{c}_{\gamma t}(k) \hat{\omega}_{\alpha\gamma}(k) \hat{\mathrm{X}}_{st}(k) - \sum_{\alpha, s} \hat{c}_{\alpha s}(k) \rho_s \hat{h}_{\alpha s}(k)\right]
\end{aligned} \tag{2.2}$$

$$\Delta\mu_{\alpha s}^{\mathrm{HNC}} = \beta^{-1} n_s \int \mathrm{d}\mathbf{r} \left(\frac{1}{2} h_{\alpha s}^2(r) - c_{\alpha s}(r) - \frac{1}{2} h_{\alpha s}(r) c_{\alpha s}(r)\right), \tag{2.3}$$

where Θ is the Heaviside function, β is the inverse temperature, n_s is the number density of site s, and $\Delta\mu_{\alpha s}^{\mathrm{HNC}}$ is the excess chemical potential using the HNC closure. When n is set to 1 in Eq. (2.2), $\Delta\mu$ corresponds to the Kovalenko–Hirata (KH) closure. $\hat{c}$, $\hat{h}$, $\hat{\omega}$, and $\hat{\mathrm{X}}$ denote the direct,

total, intramolecular correlation functions and solvent susceptibility in Fourier space. $u_{\alpha s}$ is an interaction potential between solute site α and solvent site s given as

$$u_{\alpha s}(r) = 4\varepsilon_{\alpha s}\left[\left(\frac{\sigma_{\alpha s}}{r}\right)^{12} - \left(\frac{\sigma_{\alpha s}}{r}\right)^{6}\right] + \frac{q_\alpha q_s}{r}, \tag{2.4}$$

where ε and σ are the Lennard-Jones potential parameters with conventional meanings and q_α and q_s are the effective point charge on solute site α and solvent site s, respectively.

Let us assume the HF method as the electronic structure method used in the RISM-SCF. In the HF method, the molecular orbital (MO) coefficients are the variational parameters, and the orthonormality of MOs is imposed as a constrain. The solute energy E^{U} and the constrains with the multipliers are

$$\begin{aligned} E^{\mathrm{U}} &= \mathrm{tr}\left[(\mathbf{h}^{\mathrm{core}} + \mathbf{F})\mathbf{C}\mathbf{C}^{\dagger}\right] \\ &= \mathrm{tr}[(\mathbf{h}^{\mathrm{core}} + \mathbf{F})\mathbf{D}] \end{aligned} \tag{2.5}$$

$$\boldsymbol{\zeta}^{\mathrm{U}} \cdot \boldsymbol{e}^{\mathrm{U}} = \sum_{pq} \epsilon_{pq}\left(C^{\dagger}SC - I\right)_{pq}, \tag{2.6}$$

which are common regardless of the relativistic and nonrelativistic cases. Here, matrix $\mathbf{C}$ stores the occupied MO coefficients, $\mathbf{D}$ is the density matrix, and $\mathbf{h}^{\mathrm{core}}$ and $\mathbf{F}$ are the core Hamiltonian and Fock matrices, respectively. Thus, the total Lagrangian of DHF/RISM-SCF can be rewritten as the sum of these terms, as follows.

$$\begin{aligned} L(\mathbf{C}, \boldsymbol{\zeta}_U, c, h, t) = \mathrm{tr}[(\mathbf{h}^{\mathrm{core}} + \mathbf{F})\mathbf{D}] &- \sum_{pq} \epsilon_{pq}\left(C^{\dagger}SC - I\right)_{pq} \\ &+\beta^{-1}\sum_{\alpha s} n_s \int \mathrm{d}\mathbf{r}\,[\left(1 - \Theta\left(t_{\alpha s}(r) - \beta u_{\alpha s}(r)\right)\right)\left(\exp\left(t_{\alpha s}(r) - \beta u_{\alpha s}(r)\right)\right) \\ &+\Theta\left(t_{\alpha s}(r,\lambda) - \beta\lambda u_{\alpha s}(r)\right)\left(\sum_{i=0}^{n}\frac{1}{i!}\left(t_{\alpha s}(r) - \beta u_{\alpha s}(r)\right)^{i}\right) \\ &-t_{\alpha s}(r) - h_{\alpha s}(r)t_{\alpha s}(r) + \frac{1}{2}h_{\alpha s}^{2}(r)] \\ &-\frac{\beta^{-1}}{(2\pi)^3}\int \mathrm{d}\mathbf{k}\left[\frac{1}{2}\sum_{\alpha,s,\gamma,t}\hat{c}_{\alpha s}(k)\hat{c}_{\gamma t}(k)\hat{\omega}_{\alpha\gamma}(k)\hat{\mathrm{X}}_{st}(k) - \sum_{\alpha,s}\hat{c}_{\alpha s}(k)\rho_s\hat{h}_{\alpha s}(k)\right] \end{aligned} \tag{2.7}$$

Taking variations of the Lagrangian with respect to the correlation functions $c_{\alpha s}$, $h_{\alpha s}$, and $t_{\alpha s}$ and MO coefficients $\mathbf{C}$, the stationary conditions for RISM-SCF can be obtained. The resulting equations obtained from the variations with respect to $c_{\alpha s}$, $h_{\alpha s}$, and $t_{\alpha s}$ are the RISM equations: the relational equation between the total, direct, and indirect correlation functions, and the closure equation. The equation obtained from the variation with respect to $\mathbf{C}$ is the RISM-SCF equation describing the electronic structure of the solute molecule surrounded by solvent:

$$\frac{\partial L}{\partial \mathbf{C}^\dagger} = \left(\frac{\delta E^{\mathrm{U}}}{\delta \mathbf{D}} + \frac{\delta \Delta\mu}{\delta \mathbf{D}}\right)\frac{\delta \mathbf{D}}{\delta \mathbf{C}^\dagger} - \mathbf{SC}\boldsymbol{\epsilon} = \left(\frac{\delta E^{\mathrm{U}}}{\delta \mathbf{D}} + \frac{\delta \Delta\mu}{\delta \mathbf{D}}\right)\mathbf{C} - \mathbf{SC}\boldsymbol{\epsilon} = \mathbf{0}\,, \tag{2.8}$$

where, for later convenience, the variation is taken with respect to $\mathbf{C}^\dagger$ instead of $\mathbf{C}$. The variation of E^{U} with respect to the density matrix gives the Fock matrix in gas phase:

$$\frac{\delta E^{\mathrm{U}}}{\delta \mathbf{D}} = \mathbf{F}^{\mathrm{gas}} = \mathbf{h}^{\mathrm{core}} + \mathbf{J} - \mathbf{K} \tag{2.9}$$

$$J_{\mu\nu} = \sum_{lk} D_{\sigma\lambda}(\mu\nu|\lambda\sigma) \tag{2.10}$$

$$K_{\mu\nu} = \sum_{\sigma\lambda} D_{\sigma\lambda}(\mu\sigma|\lambda\nu)\,, \tag{2.11}$$

where **J** and **K** are the Coulomb and exchange integral matrices, respectively. The variation of $\Delta\mu$ with respect to the density matrix **D** can be rewritten via the potential $u_{\alpha s}$ and the charges on the solute site, α, q_α:

$$\frac{\delta \Delta\mu}{\delta \mathbf{C}^\dagger} = \sum_{\alpha s}\frac{\delta \Delta\mu}{\delta u_{\alpha s}}\frac{\partial u_{\alpha s}}{\partial q_\alpha}\frac{\delta q_\alpha}{\delta \mathbf{D}}\frac{\partial \mathbf{D}}{\partial \mathbf{C}^\dagger} = \sum_{\mu\alpha s} q_s \int \mathrm{d}\mathbf{r}\,\frac{h_{\alpha s}(r)+1}{r} b_{\nu\mu,\alpha} C_{\mu i} = \sum_{\alpha\mu} V_\alpha b_{\nu\mu,\alpha} C_{\mu i} \tag{2.12}$$

$$V_\alpha = \sum_s \frac{\delta \Delta\mu}{\delta u_{\alpha s}}\frac{\partial u_{\alpha s}}{\partial q_\alpha} = \sum_s q_s \int \mathrm{d}\mathbf{r}\,\frac{h_{\alpha s}(r)+1}{r}\,, \tag{2.13}$$

where $b_{\mu\nu,\alpha}$ is the matrix representation of the population operator for the solute site α.

In the following, we use the relativistic four-component function as the HF wave function and derive the specific RISM-SCF equation. In the four-component method, MOs are expressed by large and small component spinors:

$$\phi_i = \begin{pmatrix} \phi_i^{\mathrm{L}} \\ \phi_i^{\mathrm{S}} \end{pmatrix}, \tag{2.14}$$

where each component is expanded by the χ basis spinors for each component:

$$\phi^{\mathrm{L}} = \sum_\mu c_{\mu i}^{\mathrm{L}} \chi_\mu^{\mathrm{L}}\,,\ \phi^{\mathrm{S}} = \sum_\mu c_{\mu i}^{\mathrm{S}} \chi_\mu^{\mathrm{S}}\,. \tag{2.15}$$

The four-component matrices can be expressed as

$$\mathbf{D} = \begin{bmatrix} \mathbf{D}^{\mathrm{LL}} & \mathbf{D}^{\mathrm{LS}} \\ \mathbf{D}^{\mathrm{SL}} & \mathbf{D}^{\mathrm{SS}} \end{bmatrix} \tag{2.16}$$

$$D_{\mu\nu}^{\mathrm{XY}} = \sum_i C_{\mu i}^{\mathrm{X}} \left(C_{\nu i}^{\mathrm{Y}}\right)^* \tag{2.17}$$

$$\mathbf{h}^{\mathrm{core}} = \begin{bmatrix} \mathbf{V}^{\mathrm{LL}} & \boldsymbol{\Pi}^{\mathrm{LS}} \\ \boldsymbol{\Pi}^{\mathrm{SL}} & \mathbf{V}^{\mathrm{SS}} - 2c^2\mathbf{S}^{\mathrm{SS}} \end{bmatrix} \tag{2.18}$$

$$V_{\mu\nu}^{\mathrm{XX}} = \langle \chi_\mu^{\mathrm{X}} | V | \chi_\nu^{\mathrm{X}} \rangle \tag{2.19}$$

$$\Pi_{\mu\nu}^{\mathrm{XY}} = \langle \chi_\mu^{\mathrm{X}} | c\boldsymbol{\sigma}\cdot\mathbf{p} | \chi_\nu^{\mathrm{Y}} \rangle \tag{2.20}$$

$$S_{\mu\nu}^{\mathrm{XX}} = \langle \chi_\mu^{\mathrm{X}} | \chi_\nu^{\mathrm{X}} \rangle \tag{2.21}$$

$$\mathbf{J} = \begin{bmatrix} \mathbf{J}^{\mathrm{LL}} & 0 \\ 0 & \mathbf{J}^{\mathrm{SS}} \end{bmatrix} \tag{2.22}$$

$$J_{\mu\nu}^{\mathrm{XX}} = \sum_{\sigma\lambda} D_{\sigma\lambda}^{\mathrm{LL}} (\chi_\mu^{\mathrm{X}} \chi_\nu^{\mathrm{X}} | \chi_\lambda^{\mathrm{L}} \chi_\sigma^{\mathrm{L}}) + D_{\sigma\lambda}^{\mathrm{SS}} (\chi_\mu^{\mathrm{X}} \chi_\nu^{\mathrm{X}} | \chi_\lambda^{\mathrm{S}} \chi_\sigma^{\mathrm{S}}) \tag{2.23}$$

$$\mathbf{K} = \begin{bmatrix} \mathbf{K}^{\mathrm{LL}} & \mathbf{K}^{\mathrm{LS}} \\ \mathbf{K}^{\mathrm{SL}} & \mathbf{K}^{\mathrm{SS}} \end{bmatrix} \tag{2.24}$$

$$K_{\mu\nu}^{\mathrm{XY}} = \sum_{\sigma\lambda} D_{\sigma\lambda}^{\mathrm{XY}} (\chi_\mu^{\mathrm{X}} \chi_\sigma^{\mathrm{X}} | \chi_\sigma^{\mathrm{Y}} \chi_\lambda^{\mathrm{Y}}) . \tag{2.25}$$

The charge q_α on solute site α in Eq. (11) is determined by the electrostatic potential (ESP) method[33,34], so as to reproduce the electrostatic potential due to the solute electron and nuclei. The vector $\mathbf{q}$ storing the point charges q_α as elements is then given by

$$\begin{aligned} \mathbf{q} = \mathrm{Tr}\left[\mathbf{D}^{\mathrm{LL}}\left(\mathbf{a}^{-1}\mathbf{B}^{\mathrm{LL}} - \frac{\left(\mathbf{1}^{\mathrm{t}}\mathbf{a}^{-1}\mathbf{B}^{\mathrm{LL}} - \mathbf{S}^{\mathrm{LL}}\right)}{\mathbf{1}^{\mathrm{t}}\mathbf{a}^{-1}\mathbf{1}}\mathbf{a}^{-1}\mathbf{1}\right)\right] \\ + \mathrm{Tr}\left[\mathbf{D}^{\mathrm{SS}}\left(\mathbf{a}^{-1}\mathbf{B}^{\mathrm{SS}} - \frac{\left(\mathbf{1}^{\mathrm{t}}\mathbf{a}^{-1}\mathbf{B}^{\mathrm{SS}} - \mathbf{S}^{\mathrm{SS}}\right)}{\mathbf{1}^{\mathrm{t}}\mathbf{a}^{-1}\mathbf{1}}\mathbf{a}^{-1}\mathbf{1}\right)\right] \end{aligned} \tag{2.26}$$

$$a_{\alpha\beta} = \int \mathrm{d}\mathbf{r} \frac{1}{|\mathbf{r} - \mathbf{R}_\alpha||\mathbf{r} - \mathbf{R}_\beta|} \tag{2.27}$$

$$B_{\mu\nu}^{XX} = \int \mathrm{d}\mathbf{r} \frac{1}{|\mathbf{r} - \mathbf{R}_\alpha|} \int \mathrm{d}\mathbf{r}' \chi_\mu^{\mathrm{X}*}(\mathbf{r}') \frac{1}{|\mathbf{r} - \mathbf{r}'|} \chi_\nu^{X}(\mathbf{r}') . \tag{2.28}$$

The variation of the site charge, Eq. (25), with respect to the density matrix gives the solvation potential matrix for solute site α:

$$\frac{\delta q_\alpha}{\delta \mathbf{D}} = \begin{bmatrix} \mathbf{b}_\alpha^{\mathrm{LL}} & \mathbf{0} \\ \mathbf{0} & \mathbf{b}_\alpha^{\mathrm{SS}} \end{bmatrix}, \tag{2.29}$$

where

$$\mathbf{b}^{\mathrm{XX}} = \mathbf{a}^{-1}\mathbf{B}^{\mathrm{XX}} - \frac{\left(\mathbf{1}^{\mathrm{t}}\mathbf{a}^{-1}\mathbf{B}^{\mathrm{XX}} - \mathbf{S}^{\mathrm{XX}}\right)}{\mathbf{1}^{\mathrm{t}}\mathrm{a}^{-1}\mathbf{1}}\mathbf{a}^{-1}\mathbf{1}. \tag{2.30}$$

The solvation Fock matrix is defined as the sum of the gas-phase Fock matrix and solvation potential matrix:

$$\mathbf{F}^{\mathrm{solv}} = \begin{bmatrix} \mathbf{F}^{\mathrm{LL,gas}} + \mathbf{V}^{\mathrm{LL,solv}} & \mathbf{F}^{\mathrm{LS,gas}} \\ \mathbf{F}^{\mathrm{SL,gas}} & \mathbf{F}^{\mathrm{SS,gas}} + \mathbf{V}^{\mathrm{SS,solv}} \end{bmatrix}, \tag{2.31}$$

where

$$\mathbf{V}^{\mathrm{XX,solv}} = \sum_\alpha V_\alpha \mathbf{b}_\alpha^{\mathrm{XX}} . \tag{2.32}$$

Thus, we finally obtain the DHF/RISM-SCF equation as an eigenvalue problem:

$$\mathbf{F}^{\mathrm{solv}}\mathbf{C} = \mathbf{S}\mathbf{C}\boldsymbol{\epsilon}. \tag{2.33}$$

Due to the variational formalism, energy derivatives, in particular first-order derivatives, can be concise, as shown by Sato et al.[31] The first-order derivative of the Helmholtz energy with respect to the solute molecular coordinates $\mathbf{R}_a$ is expressed simply as

$$\frac{\partial A}{\partial \mathbf{R}_a} = \frac{\partial E^{\mathrm{U}}}{\partial \mathbf{R}_a} + \frac{1}{2\beta(2\pi)^3} \sum_{\alpha\gamma st} \int \mathrm{d}\mathbf{k}\, \hat{c}_{\alpha s}(k)\hat{c}_{\gamma t}(k) \frac{\partial \hat{\omega}_{\alpha\gamma}(k)}{\partial \mathbf{R}_A} \hat{\mathrm{X}}_{st}(k) + \sum_{\alpha} V_\alpha \mathrm{tr}\left(\mathbf{D}\frac{\partial \mathbf{b}_\alpha}{\partial \mathbf{R}_A}\right). \quad (2.34)$$

The first term of the right-hand side of Eq. (2.34) corresponds to the change in the solute electronic energy; the second term corresponds to the change in the solute–solvent distribution function due to the modification of the intramolecular correlation; and the last term corresponds to the change in partial charge on solute sites. The analytical energy gradients for the four-component relativistic DHF/RISM-SCF are obtained by replacing the nonrelativistic molecular integral with four-component ones.

2.3 Computational details

To demonstrate the present method, we applied it to the ground states of the I^- ion, to methyl iodide CH_3I, and to hydrogen chalcogenides H_2X (X = O, S, Se, Te, and Po) in aqueous solution. The basis sets used in the DHF calculations were the uncontracted correlation-consistent valence triple zeta (cc-pVTZ) basis set for C, H, O, and S[35,36], and the uncontracted Dyall's triple zeta plus polarization (TZP) basis set for Se, Te, I, and Po.[37] The geometries of CH_3I and H_2X in the solution were optimized at the DHF/RISM-SCF level.

The parameters used in the RISM-SCF method were as follows. The temperature and density of solvent water were 298 K and 0.03334 molecules $Å^{-3}$, respectively. The LJ parameters σ and ε for the solute and solvent sites are listed in Table 1.[38] For H_2Po, the LJ parameters for the H of silane (H_4Si) were used[39] to ensure proper charge polarization between H and Po. The transferable intermolecular potential with three points (TIP3P) parameter set[40] for the geometrical and potential parameters for solvent water was used with modified H parameters. There were 2048 grid points with a spacing of 0.05 Å for pair correlation functions in the RISM calculations. PCM-SCF calculations were performed by DIRAC19.[41],[42]

2.4 Applications

2.4.1 The iodine ion (I^-) and methyl iodide (CH_3I)

The electronic structure and solvation structure of the iodine ion (I^-) and methyl iodide (CH_3I) were evaluated by the relativistic and nonrelativistic HF/RISM-SCF methods. In Table 2, the Helmholtz energy and its components obtained by relativistic and nonrelativistic methods for I^- and CH_3I are compared.

The solvation free energy (SFE) A^{slv} in the RISM-SCF method is defined as the difference between the Helmholtz energy in solution phase A and the energy in the gas phase E^{gas}:

$$A^{\mathrm{slv}} = A - E^{\mathrm{gas}} = E^{\mathrm{U}} - E^{\mathrm{gas}} + \Delta\mu. \quad (2.35)$$

The energy difference, $E^{\mathrm{U}} - E^{\mathrm{gas}}$, in the right-hand side can be regarded as the electronic reorganization energy E^{reorg} due to the solvation, and the excess chemical potential $\Delta\mu$ can be divided into the electrostatic $\Delta\mu^{\mathrm{ES}}$ and the nonelectrostatic $\Delta\mu^{\mathrm{NES}}$ components; hence, A^{slv} is further rewritten as

$$A^{\mathrm{slv}} = E^{\mathrm{reorg}} + \Delta\mu^{\mathrm{ES}} + \Delta\mu^{\mathrm{NES}}. \quad (2.36)$$

As shown in Table 2.2, I^- is strongly stabilized due to the solvation because of its ionic nature. The major contribution to this stabilization is the electrostatic interaction with the solvent water. Since I^- consists of only one site, all the electron charges are assigned to the single site. As a result, the solute–solvent interaction potential for the RISM calculation is the same in both relativistic and nonrelativistic calculations. Therefore, the SFE values are identical in both cases. By contrast, the SFE of CH_3I, a polyatomic molecule, is affected by the relativistic effects. In the DHF/RISM-SCF framework, the relativistic effects on electronic states of the solute molecule influence the solute–solvent interactions through effective charges on solute atoms. Moreover, the solvation structure changed by relativistic effects also affects the electron reorganization energy of the solute molecule. In the present calculation, the relativistic effects seem to suppress the electrostatic interaction between solute and solvent molecules and therefore the magnitude of all the SFE components becomes smaller than those of nonrelativistic results. Consequently, the total SFE of the relativistic calculation, 11.96 kcal mol^{-1}, was slightly lower than the nonrelativistic one, 12.00 kcal mol^{-1}. The optimized molecular structure and electrical properties of solute CH_3I are summarized in Table 2.3. As can be seen in the table, the C–I distance and the dipole moment of the solute CH_3I become smaller due to the relativistic effects. Such structural and electrostatic character weakens the solute–solvent interactions.

The radial distribution functions (RDFs)[43] between the I ion/atom of the solute and the O and H atoms of the solvent by DHF/RISM-SCF are shown in Figure 1. For I^-, the RDF for I–O has a sharp high peak at r = 3.4 Å and the RDF for I–H has a sharp high peak at r = 2.15 Å and a relatively low peak at r = 4.15 Å. In CH_3I, the RDF for I–O has a high peak at r = 3.50 Å, and the RDF for I–H has a shoulder around r = 2.70 Å and a peak at r = 4.20 Å. These peaks and the shoulder correspond to water molecules in the first solvation shell. The peaks of CH_3I are featured to be lower and broader than those of I^-. These results indicate tight hydration around the charged I^- ion and loose hydration around I of the neutral molecule CH_3I.

The difference between the RDFs of CH_3I by the relativistic and nonrelativistic RISM-SCF is shown in Figure 2.2. The RDFs of I^- are not shown because they are identical for relativistic and nonrelativistic, as discussed above. From the figure, the first peak height of the RDF in the relativistic case is slightly lower than in the nonrelativistic case. This feature corresponds to the SFE behavior discussed above; i.e., the introduction of the relativistic effects weakens the solute–solvent interaction.

In contrast to the solvation structures, which differ little between the relativistic and nonrelativistic cases, the electronic structures of I^- and CH_3I are naturally different due to the relatively large spin–orbit interaction. Figure 2.3(A) and (B) present the energy levels of the four highest energy orbitals (including degeneracy) of I^- and CH_3I, respectively. In the charged system I^-, the $5p_{3/2}$, $5p_{1/2}$ and 5s orbitals are significantly stabilized by −0.2989. The MOs of CH_3I corresponding to these orbitals of I^- are the highest occupied MO (HOMO) (9e; characterized as $5\pi_I$), HOMO−1 ($9e'$; $5\pi_I'$), HOMO−2 ($13a_1$; σ_{CH}), and HOMO−5 ($12a_1$; $5s_I$). The stabilizations of these energy levels are relatively small, namely: −0.0346, −0.0338, *z*, and −0.0290 a.u., respectively, as expected for a neutral molecule.

2.4.2 Hydrogen chalcogenide H_2X (X = O, S, Se, Te, and Po)

Another example is the series of hydrogen chalcogenides. The structural parameters of the H_2X molecules in the gas phase and in water, which were optimized using the DHF/RISM-SCF and DHF/PCM-SCF methods, are shown in Table 4. These molecules have also been examined in the relativistic PCM-SCF study.[23] This study reported that bond lengths increase monotonically with increasing chalcogen atomic number in correlation with the size of the central atom, and that there is no deviation from this trend even when relativity is included and the solvent effect is considered. The DHF/RISM-SCF method provides similar results. The structures by DHF/RISM-SCF and DHF/PCM-SCF methods in the table are quite close to each other, with a maximum difference of 0.04 Å in bond distance and 2.5° in bond angle. For the bond distance, the DHF/RISM-SCF method tends to have a slightly larger distance, and for the bond angle, the DHF/RISM-SCF method tends to have a slightly smaller angle. The solvent effect on the solute structure was smaller with the DHF/RISM-SCF method than with DHF/PCM-SCF. In fact, even for H_2O, where the change in electric dipole moment due to solvation, as will be shown later, is large: the changes are +0.005 Å for bond distance and −0.3° for bond angle. This is much the same for the DHF/PCM-SCF method.

The Helmholtz energies, as well as the SFEs and their components, for H_2X (X = O, S, Se, Te, and Po) are shown in Table 2.5. The Helmholtz energies and SFEs by the DHF/PCM-SCF method are also listed. The nonelectrostatic contributions to the SFEs were not included because

the nonelectrostatic energy is not handled in the current PCM implementation of the program package (DIRAC). Hence, the SFEs by the DHF/PCM-SCF method are the sum of E^{reorg} and $\Delta\mu^{\mathrm{ES}}$. For this reason, direct comparison between the total SFEs A^{slv} by the DHF/PCM-SCF and DHF/RISM-SCF methods is not appropriate, and only the electrostatic and electronic reorganization energies are compared below. Table 2.6 lists the *z* components of the electric dipole moments and the electrostatic potential (ESP) charge on the X atom of the solute molecule. The H_2X molecules have a C_{2v} symmetry, and thus only the *z* component of the dipole moment has a value.

The SFE by the DHF/RISM-SCF method is negative (−5.31 kcal/mol) for H_2O and positive (6.95–14.94 kcal/mol) for the other molecules, increasing with the atomic number of chalcogen. The electrostatic and nonelectrostatic components of the SFE increase from H_2O to H_2Po: the electrostatic component increases from −18.17 kcal/mol for H_2O to −0.22 for H_2Po, and the nonelectrostatic component increases from 6.82 kcal/mol for H_2O to 15.07 for H_2Po. By contrast, the reorganization energy, is smaller than these two energies, decreasing from 6.04 to 0.99 kcal/mol. According to Table 6, the magnitude of the electric dipole moment and ESP charge decrease with increasing chalcogen atomic number, indicating that the polarity of the molecules reduces with increasing chalcogen atomic number. The SFE results correspond to the magnitude of the molecular polarity. That is, the larger the polarity of the molecule, the larger the magnitude of the electrostatic component and the reorganization energy, and the smaller the magnitude of the nonelectrostatic component. For H_2O, the most polar molecule, the electrostatic component of –18.17 kcal/mol is dominant, and the nonelectrostatic component and reorganization energy are of similar magnitude, 6.82 and 6.04 kcal/mol, respectively. By contrast, for H_2Po, the least polar molecule, the nonelectrostatic energy of 15.07 kcal/mol is dominant, and the electrostatic component and reorganization energy are very small, −0.22 and 0.09 kcal/mol, respectively. Both the electrostatic component and reorganization energy are rather smaller by the DHF/PCM-SCF method than by the DHF/RISM-SCF method. Even for H_2O, which has the largest magnitude, the electrostatic component and reorganization energy are −6.28 and 0.67 kcal/mol, respectively. Note that comparing the dipole moments of RISM and PCM in Table 6, the DHF/RISM-SCF values are larger than those of DHF/PCM-SCF. The maximum difference is 0.306 a.u. for H_2Se, while the difference is relatively small for H_2Po with different polarity, 0.015 a.u. The overestimation may be attributed to the fact that the RISM-SCF method overestimates the polarization of solute molecules in polar solvents when using the point-charge representation.[44]

The RDFs by the DHF/RISM-SCF method are shown in Figure 4(A)–(D). The RDFs of

H_2S, H_2Se, and H_2Te were similar, indicating that the RDF features can be classified into three groups: H_2O, H_2S–H_2Te, and H_2Po. In all the RDFs, the peak heights decrease with increasing chalcogen atomic number. This reflects the fact that the solute–solvent interaction weakens with increasing chalcogen atomic number, as can be seen from the polarity of the solute molecules in Table 6.

The RDF, $g_{\mathrm{X-H}}$, between X of the solute and H of the solvent (Figure 4(A)) shows a conspicuous peak at 1.80 Å for H_2O, but there are no corresponding peaks for the other molecules; the second peak for H_2O corresponds to the first peaks of the other molecules. These first peaks are at shorter distances than the first RDF peak between X of the solute and O of the solvent (Figure 4(B)) in the case of H_2O–H_2Te, and at about the same distance for H_2Po. This indicated that for H_2O, there is distinct hydrogen bond formation between O of the solute and H of the solvent; for H_2Po, the solvent waters take a nearly random orientation with respect to Po; and for H_2S, H_2Se, and H_2Te, the solvent waters are roughly oriented with H toward the X of the solute.

For the four molecules H_2O–H_2Te the RDFs, $g_{\mathrm{H-O}}$, between H of the solutes and O of the solvent in Figure 4(D) have a peak at about 2 Å, and the RDFs, $g_{\mathrm{H-H}}$, between H of the solute and H of the solvent in Figure 4(C) have a peak or shoulder at about 2.5 Å. These indicate the hydrogen bond formation between solute H and solvent O for the three molecules. In contrast, there is no peak at a similar position in H_2Po, and $g_{\mathrm{H-O}}$ has a small peak around $r = 3.1$ Å, indicating that H of the solute and O of solvent are loosely bound without forming an obvious hydrogen bond.

2.5 Conclusions

We have presented the DHF/RISM-SCF method, which is the initial implementation of a combined method of a four-component relativistic theory and an integral equation theory of molecular liquid to consider both the relativistic and the solvent effects on the electronic structure of solvated molecules. The method was formulated as a variational form of the Helmholtz energy, and the analytic energy gradients were also derived using the variational property.

We have applied the DHF/RISM-SCF method to iodine ion I^-, methyl iodide CH_3I, and hydrogen chalcogenide H_2X (X = O–Po) in aqueous solutions. For I^- and CH_3I, the SFEs and their components, and the RDFs of solvent around the I atoms were shown and discussed. For species with no or small charge bias, the absolute reorganization energy was very small, and the signs of the SFEs were determined by the electrostatic energy in $\Delta\mu$ for I^- and by the

nonelectrostatic energy in $\Delta\mu$ for CH_3I. The solvation structures for I^- and CH_3I around the I atom were similar for the peak and shoulder positions, whereas the peak heights were different due to the charge differences. The comparison with the nonrelativistic HF/RISM-SCF results indicated that changes in solvation structure due to relativistic effects were relatively small. In contrast, for the electronic structures of solute, such as the orbital energy levels, the relativistic description using the DHF/RISM-SCF method was essential. For H_2X, the molecular structures, SFE and their components, the electric dipole moment and ESP charges of the solute, and the RDF of solvent around the X and H atoms were computed and discussed focusing mainly on the differences due to the heavy atom X. As shown by the dipole moment results, the polarity of molecule decreased with increasing chalcogen atomic number. Consequently, the SFE increased, and the electrostatic energy decreased in its absolute value. The solvation structures of H_2X were classified into three groups: H_2O, H_2S–H_2Te, and H_2Po. In H_2O, both the O and H atoms formed hydrogen bonds with solvent water. In H_2Po, by contrast, the solvent water took nearly random orientations around the Po atom of the solute. The H atom of the solute and the O atom of the solvent were loosely bound without forming an obvious hydrogen bond. In other molecules, hydrogen bond formation was observed between the H of the solute and the O atom of the solvent, and the solvent waters were roughly oriented with the H atom toward the heavy element of the solute. Overall, it can be said that the DHF/RISM-SCF method appropriately introduces solvent effects to the four-components relativistic electronic structure theory.

The present DHF/RISM-SCF method can be extended in both the four-component relativistic electronic structure theory of solute molecules and the solvent model. Though the electron correlation effect is not so large for the molecular systems treated in the present article, the combination with electron correlation methods is crucial, especially for the precise description of the electronic structure of solute molecules, the quantitative description of chemical reactions, and their application to quasidegenerate systems. For full variational electronic structure methods, such as the four-component KS-DFT and MCSCF methods, the variational approach to the Helmholtz energy is applicable, as described in the Methods section. Additionally, for nonvariational electron correlation methods, such as the four-component perturbation and coupled-cluster methods, the formulation procedure using a Lagrangian in the RISM-SCF method is now well established. For solvent models, more accurate models such as three-dimensional (3D) RISM[45,46] and the molecular Orenstein–Zernike (MOZ)[47,48] model that are compatible with the four-component relativistic method describing fine electronic structures of solutes, are desired. The 3D-RISM theory explicitly incorporates the orientation of one molecule in the two-body interaction between molecules, and the MOZ

theory explicitly incorporates the orientations of both molecules, resulting in the 3D-RISM-SCF[49]·[50] and MOZ-SCF[51]·[32] methods using these models to refine the description of solute–solvent intermolecular interactions. Those developments are currently in progress.

Table 2.1 LJ parameters of solute and solvent sites used in the RISM-SCF calculations

	σ / Å	ε / kcal mol^{-1}	q / e[a]
I^- and CH_3I			
C	3.3997	0.1094	–
H	2.4714	0.0157	–
I	3.8309	0.5	–
H_2X (X=O–Po)			
H (expect for H_2Po)	1.0000	0.056	–
H (for H2Po)	2.886	0.325	–
O	3.166	0.1554	–
S	4.035	0.274	–
Se	4.205	0.291	–
Te	4.009	0.339	–
Po	4.709	0.325	–
Solvent water			
O	3.166	0.1554	−0.8476
H	1.0000	0.056	0.4238

[a] The partial charges on solute sites are determined as a result of the RISM-SCF calculation.

Table 2.2 Helmholtz energy and solvation free energy for I− and CH3I, and their component decomposition

	I^-		CH_3I	
	Relativistic	Nonrelativistic	Relativistic	Nonrelativistic
A / Hartree	−7116.25060	−6918.21333	−7155.65459	−6957.60014
E^U	−7116.11102	−6918.07374	−7155.67243	−6957.61794
$\Delta\mu$	−0.13959	−0.13959	0.01784	0.01780
A^{slv} / kcal mol^{-1}	–87.59	–87.59	11.96	12.00
$\Delta\mu^{NES}$	7.30	7.30	14.40	14.41
$\Delta\mu^{ES}$	–94.89	–94.89	–3.21	–3.24
E^{rorg}	$< 10^{-3}$	$<10^{-3}$	0.76	0.83

Table 2.3 Optimized geometrical parameters, *z* component of electric dipole moment, and ESP charge for CH_3I

	Relativistic		Nonrelativistic	
	GAS	RISM	GAS	RISM
r(C–I) / Å	2.143	2.155	2.144	2.157
r(C–H) / Å	1.075	1.073	1.075	1.073
∠ICH / degree	107.5	106.6	107.7	106.7
DM(z) / a.u.	−0.763	−1.080	−0.821	−1.155
q_I / e	−0.128	−0.185	−0.146	−0.210
q_C / e	−0.402	−0.495	−0.344	−0.378
q_H / e	0.177	0.226	0.164	0.196

Table 2.4 Optimized geometrical parameters for H2X (X = O–Po)

	GAS		RISM		PCM	
X	*r* / Å	*θ*/ degree	*r* / Å	*θ* / degree	*r* / Å	*θ* / degree
O	0.940	105.9	0.945	105.6	0.944	104.9
S	1.329	94.1	1.330	96.1	1.331	94.9
Se	1.451	92.9	1.449	95.2	1.452	93.7
Te	1.649	92.1	1.645	93.9	1.649	92.6
Po	1.742	90.7	1.742	90.3	1.746	90.0

Table 2.5 Helmholtz energy and solvation free energy for H_2X (X = O–Po), and their component decomposition

	H_2O		H_2S		H_2Se		H_2Te		H_2Po	
	RISM	PCM	RISM	PCM	RISM	PCM	RISM	PCM	RISM	PCM
A / Hartree	–76.1209	–76.1218	–399.8201	–399.8352	–2429.7964	–2429.8143	–6795.0666	–6795.0840	–22238.6862	–22238.7121
E^{U}	–76.1041	–76.1118	–399.8269	–399.8306	–2429.8077	–2429.8106	–6795.0794	–6795.0813	–22238.7099	–22238.7093
$\Delta\mu$	–0.0167	–0.0100	0.0068	–0.0046	0.0113	–0.0037	0.0127	–0.0027	0.0237	–0.0028
A^{slv} / kcal mol^{-1}	–5.31	–5.61	6.95	–2.53	9.13	–2.06	8.78	–1.59	14.94	–1.61
$\Delta\mu^{NES}$	6.82	-	10.48	-	11.27	-	9.46	-	15.07	-
$\Delta\mu^{ES}$	–18.17	–6.28	–6.36	–2.90	–4.38	–2.32	–1.67	–1.72	–0.22	–1.75
E^{rorg}	6.04	0.67	2.83	0.37	2.24	0.25	0.99	0.13	0.09	0.14

Table 2.6 *z* Component of electric dipole moment and ESP charge on X for H_2X (X = O–Po)

	H_2O	H_2S	H_2Se	H_2Te	H_2Po
GAS					
DM(*z*) / a.u.	0.781	0.449	0.307	0.115	–0.229
q / *e*	–0.741	–0.319	–0.226	–0.116	0.033
RISM					
DM(*z*) / a.u.	1.137	0.861	0.732	0.464	–-0.342
q / *e*	–1.056	–0.553	–0.446	–0.268	0.080
PCM[a]					
DM(*z*) / a.u.	0.903	0.584	0.426	0.191	–0.327

[a] Reference 23.

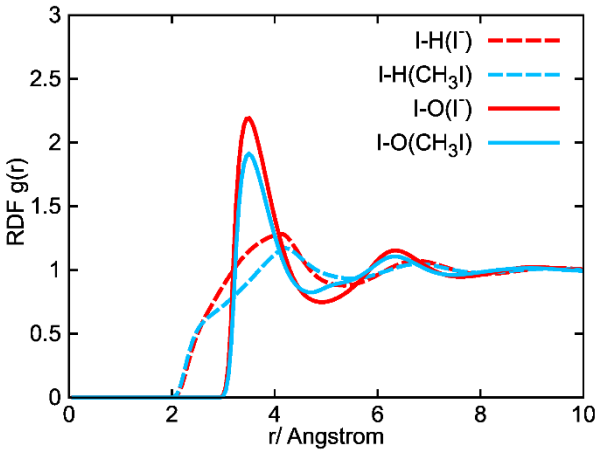

Figure 2.1 Radial distribution functions between the I atom and solvent water

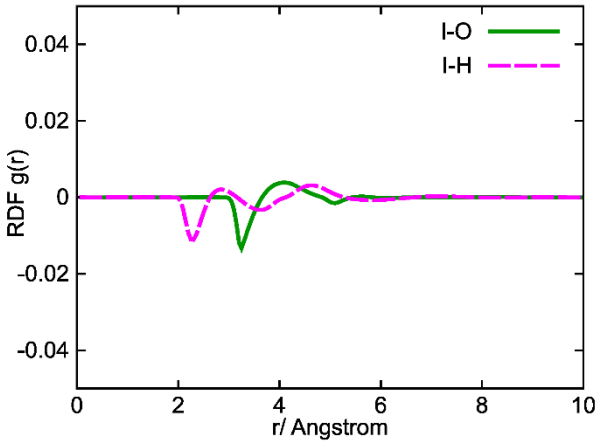

Figure 2.2 Difference between the relativistic and nonrelativistic radial distribution functions for CH_3I

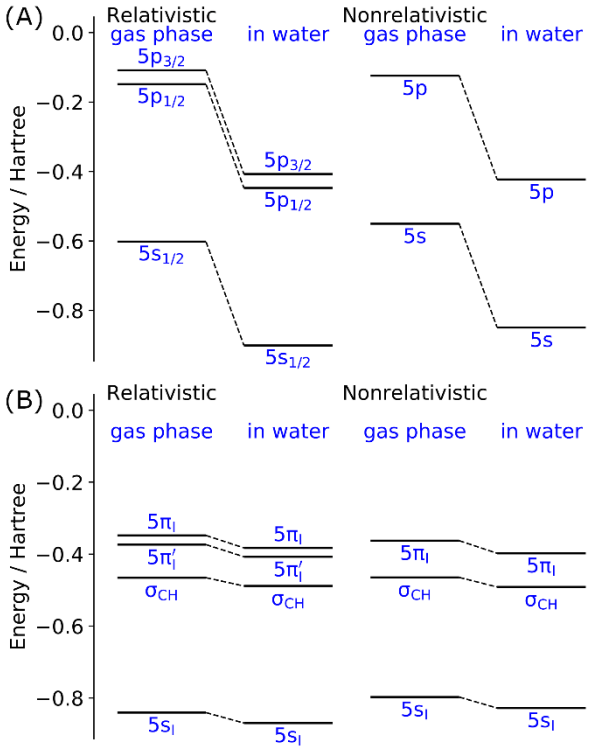

Figure 2.3 Energy levels of (A) 5p orbitals of I^- and (B) 5p orbitals of I in CH_3I

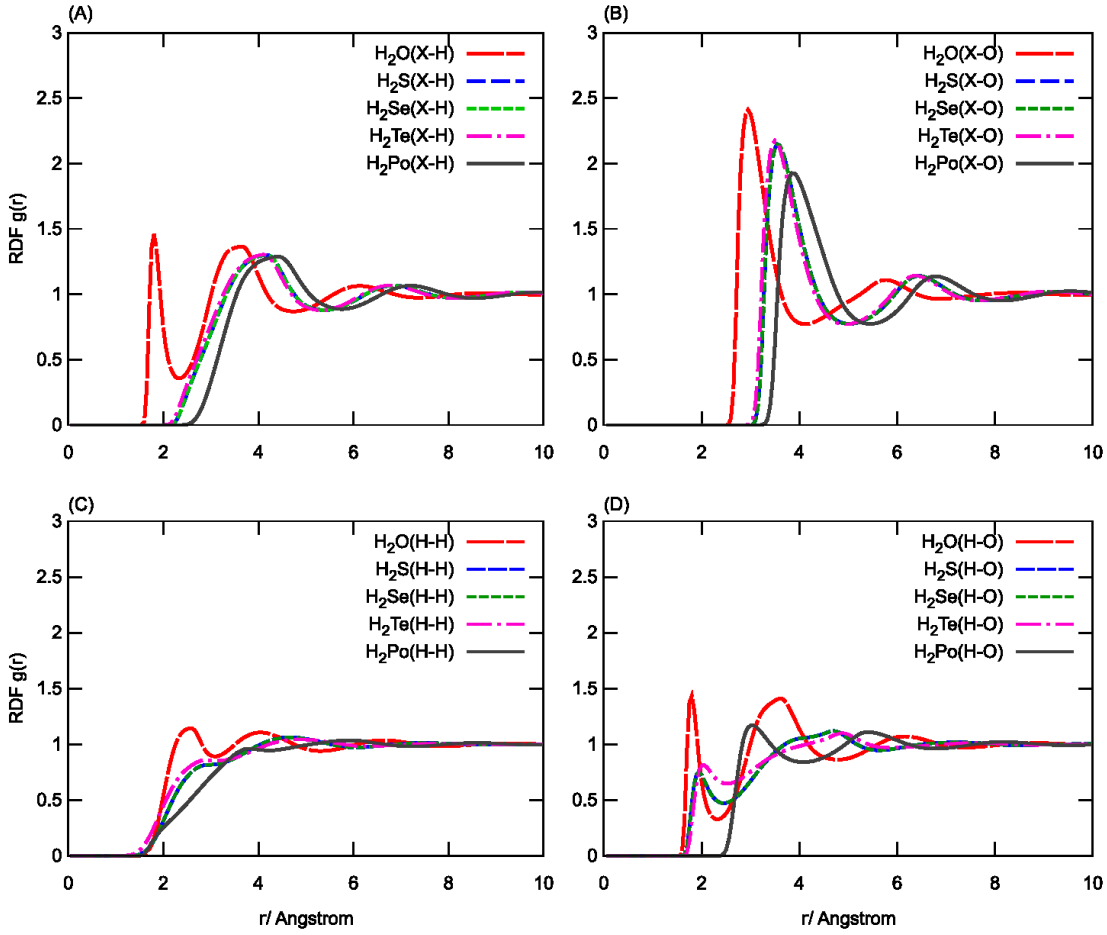

Figure 2.4 Radial distribution functions between H2X and solvent water

Chapter 3.

Application of reference interaction site model self-consistent field method based on Dirac–Hartree–Fock wave function to chemical reaction

3.1 Introduction

For the electronic structure of molecules containing heavy elements, relativistic effects play an important role. Nowadays it is widely known that both the scalar and spin-orbit effects are important for the geometries and properties of molecules. There are several methods to treat these relativistic effects theoretically. Among them, the four-component method[52] based on the Dirac equation is one of the most suitable methods for treating relativistic effects because it is based on the basic equation of relativistic quantum mechanics. Therefore, many methods for describing electronic structure, including the electron correlation methods, have been transferred to the relativistic four-component level.

For molecules in the solution phase, solvent effects also play an important role. Among the various solvation models, the polarizable continuum model (PCM)[53,54] is one of the most widely used approaches. In the PCM approach, the solvent molecules are considered as a continuum medium. In 2015, Di Remigio et al.[23] presented a formulation of four-component relativistic self-consistent field (SCF) theory for a molecular solute described within the PCM for solvation, and successfully applied to systems heavy-element containing. However, the PCM approach lacks microscopic solute–solvent interactions such as hydrogen bonds. A method that can handle such microscopic interactions is the reference interaction site model self-consistent field (RISM-SCF) method[29,30], which combines the electronic structure theory with the reference interaction site model[28,43], an integral equation theory of molecular liquids.

In chapter 2, we have proposed the RISM-SCF based on the Dirac–Hartree–Fock (DHF) method, one of the four-component relativistic molecular orbital methods. This method can simultaneously calculate the precise electronic structure of molecules, including relativistic effects, with the DHF method and the solvent structure with the RISM theory. In this chapter, we present the application of this method to a chemical reaction involving heavy atoms, namely, a Menshutkin reaction $NH_3 + CH_3I \rightarrow NH_3CH_3^+ + I^-$ in aqueous solution.

3.2 Computational detail

Reaction coordinate d of this reaction was defined as the difference between internuclear distance between carbon and iodide $r_{\mathrm{C-I}}$ and internuclear distance between carbon and nitrogen $r_{\mathrm{C-N}}$:

$$d = r_{\mathrm{C-I}} - r_{\mathrm{C-N}} \tag{3.1}$$

To construct free energy surface along the reaction coordinate, constrained geometry optimization was performed at non-relativistic HF/cc-PVDZ-PP level with fixed reaction coordinate. Then, single point energy calculation was performed at each geometry by DHF/PCM-SCF and DHF/RISM-SCF. To including solvent effects in reaction coordinate, solvation model based on density (SMD) [55] was employed in constrained geometry optimization. Lennerd-Jones parameters are shown in Table 3.1. The basis sets used in the DHF calculations were the uncontracted Dyall's double zeta basis for iodide and uncontracted correlation-consistent valence double zeta (cc-pVDZ) for other elements.

3.3 Results and discussion

Figure 3.1(A) shows the Helmholtz energies A along the reaction coordinate d by the DHF/RISM-SCF and DHF/PCM-SCF methods, where A is shifted so that the energy of the reactant NH_3 + CH_3I in gas phase is zero. RISM-SCF gives a larger Helmholtz energy than PCM-SCF on the reactant side, while giving a smaller Helmholtz energy on the product side. The reaction is exergonic, and the reaction free energies are 47.37 kcal mol^{-1} and 33.42 kcal mol^{-1} for RSIM-SCF and PCM-SCF, respectively. Solvent effects decrease activation free energy and TS more reactant side. This is because the solutes are ionized in the product state due to charge separation, which enhances the solute-solvent interaction and stabilizes the product state. RISM describes hydrogen bonds between solutes and solvents well, however PCM underestimates them, therefore RISM has a greater stabilization of the product state compared with the PCM case. Due to the larger reaction free energy, the transition state (TS) of RISM-SCF is located more on the reactant side than that of PCM-SCF, at $d = 0.0$ Å for RISM-SCF and at 0.3 Å for PCM-SCF. The activation free energies are 7.23 and 12.94 kcal $amol^{-1}$ for RISM- and PCM-SCF, respectively. Note that the activation energy, 23.5 kcal mol^{-1}, determined by kinetic analysis, was reported for this reaction by Okamoto et al.[56,57] although it is different from the activation *free* energy and therefore cannot be directly compared.

Figure 3.1(B) shows the components of A by RISM-SCF, where $\boldsymbol{E^{gas}}$ is shifted so that $\boldsymbol{E^{gas}}$ of the reactant is zero. $\boldsymbol{E^{gas}}$ has a very shallow first minimum and a second minimum, corresponding to the dipole-bound complex and ion pair, respectively, as usual Menshutkin reaction profiles in the gas phase show. The very shallow first minimum is due to the very small dipole moment of CH_3I. This energy is destabilized by the nearly constant $\boldsymbol{\Delta\mu^{NES}}$ and by $\boldsymbol{E^{reorg}}$

while stabilized by $\boldsymbol{\Delta\mu^{ES}}$. The stabilization by $\boldsymbol{\Delta\mu^{ES}}$ is particularly pronounced after TS, where the charges are separated. Table 3.2 shows the Helmholtz energies *A* by RISM-SCF and their components at the reactant, TS (d = 0.0 Å), and the product. In the reactant, which is a pair of neutral molecules, $\boldsymbol{E^{reorg}}$ and $\boldsymbol{\Delta\mu^{ES}}$ are relatively small (3,88 and −13.55 kcal mol^{-1}, respectively) and $\boldsymbol{\Delta\mu^{NES}}$ is dominant (21.93 kcal mol^{-1}). In the TS, $\boldsymbol{E^{gas}}$ increases relative to the reactant (11.17 kcal mol^{-1}) and $\boldsymbol{E^{reorg}}$ also increases in response to the increase in charge bias (8.89 kcal mol^{-1}). $\boldsymbol{\Delta\mu^{ES}}$ also becomes large (−21.90 kcal mol^{-1}) as in $\boldsymbol{E^{reorg}}$, but is still comparable to $\boldsymbol{\Delta\mu^{NES}}$ (21.33 kcal mol^{-1}) because the charges are not sufficiently well separated. This may be due to the fact that the TS is on the reactant side in the Helmholtz energy profile. In contrast, in the product, $\boldsymbol{E^{gas}}$ increases significantly (95.27 kcal mol^{-1}) due to charge separation, while $\boldsymbol{E^{reorg}}$ is relatively small (0.87 kcal mol^{-1}) because the system has already been separated into ions. In the product, which is a pair of ions, $\boldsymbol{\Delta\mu^{ES}}$ is very large (−152.50 kcal mol^{-1}) and greatly stabilizes the system, outweighing the destabilization of $\boldsymbol{E^{gas}}$.

The data in the figures and the table as a whole well illustrate the characteristics of the Menshutkin reaction, which is endergonic due to the charge separation and shows a late TS in the gas phase, but results in an early TS due to the large stabilization of the ionic product by the solvent.

3.4 Conclusion

We have presented an application of the RISM-SCF method, based on four-component relativistic electronic structure theory, to a chemical reaction. We constructed Helmholtz energy profiles of a Menshutkin reaction $NH_3 + CH_3I \rightarrow NH_3CH_3^+ + I^-$ and conducted component analysis. The reaction profile by the RISM-SCF method well described the characteristics of the Menshutkin reaction, and the component analysis revealed the contributions of the effects of electron reorganization and electrostatic and non-electrostatic interactions. The DHF/RISM-SCF method has proven to be one of the effective methods for analyzing chemical reactions of systems containing heavy atoms such as iodine. Although the current method does not include the electron correlation effect in molecules, the development of RISM-SCF based on four-component electron correlation methods is in progress.

Table 3.1 LJ parameters of solute and solvent sites used in the RISM-SCF calculations

	σ / Å	ε / kcal mol^{-1}	q / e[a]
NH_3 and CH_3I			
C	3.3997	0.1094	–
H(CH3)	2.4714	0.0157	–
I	3.8309	0.5000	–
N	3.2500	0.1700	–
H(NH3)	1.0691	0.0157	–
Solvent water			
O	3.166	0.1554	−0.8476
H	1.0000	0.056	0.4238

[a] The partial charges on solute sites are determined as a result of the RISM-SCF calculation.

Table 3.2 Helmholtz energies and their components at the reactant, TS, and product (kcal mol^{-1})

	Reactant		TS	Product	
	Total	NH_3 + CH_3I	NH_3–CH_3–I	Total	$NH_3CH_3^+$ + I^-
A [a]	12.26	−0.34 +12.60	19.49	−35.11	
Component					
E^{gas} [a]	0.00		11.17	95.27	
E^{reorg}	3.88	3.15 +0.73	8.89	0.87	0.87 +0.00
$\Delta\mu^{NES}$	21.93	7.46 +14.47	21.33	21.25	13.95 +7.30
$\Delta\mu^{ES}$	−13.55	−10.95 −2.60	−21.90	−152.50	−57.60 −94.89

[a] The values of A and E^{gas} are shifted so that the energy of the reactant in the gas phase E^{gas}(R) is zero. E^{gas}(R) = −7211.8716 a.u.

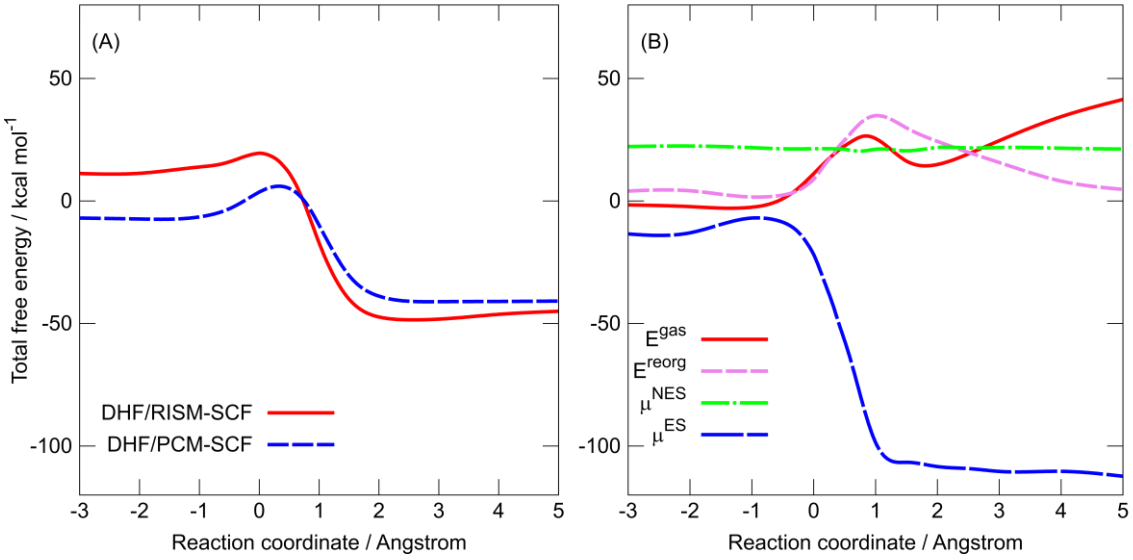

Figure 3.1 (A)Helmholtz energy profiles of RISM- and PCM-SCF and (B) energy components of RISM-SCF

Chapter 4.

Relativistic two-component method based on quasi-degenerate perturbation theory

4.1 Introduction

The relativistic effects are most naturally incorporated by the four-component methods based on the Dirac equation. However, in many quantum chemical calculation today, the relativistic two-component methods are also often used due to high computational cost of four-component method. The concept of two-component method is separation of electronic and positronic states. The Dirac equation gives four-component spinors as solutions describing the electrons and their anti-particles, the positrons. The components of the four-component spinors can be classified into large and small parts, each of which is characterized by a large and a small contribution to the electronic solution. Treating all the four components is highly expensive in computational cost. Comparing with four-component method, two-component method treat explicitly only two-component which is half of four-component. The two-component spinors used in this method are transformed spinors that are decoupled from the degrees of freedom of positrons and thus are not identical to any parts of the original four components.

The decoupling transformation of the one-electron Hamiltonian, on which the two-component method is based, has extra degrees of freedom and tis not determined uniquely. Therefore, various versions of the two-component method has been proposed until now: the Breit–Pauli approximation (BPA) , the zeroth-order and infinite-order regular approximation (ZORA, IORA) [58,59], the relativistic scheme for eliminating small components (RESC) [60], the Douglas–Kroll (DK) method[61–66], the infinite-order two-component (IOTC) method[67], and the exact-two-component (X2C) method[68,69]. These methods are now equipped in several program packages and are commonly used in the studies in this field. Transforming four-component Hamiltonian to two-component Hamiltonian cause inherit error called the picture-change error or effects (PCE). PCE is an artificial error in the two-component method originating from the inconsistency of the basis between operators. PCE significantly affects molecular properties relevant to inner-shell region electron density, such as the nuclear magnetic shielding tensor used in chemical shift calculations.

The Douglas–Kroll (DK) method is a method based on a multistep transformation. This method is an effective method, but the conventional DK scheme has a problem of computational

cost. A main source of the computational cost is the total unitary transformation, which is expressed as a product of unitary matrices. An alternative DK scheme with polynomial cost was proposed by Peng and Hirao[70]. In this scheme, unitary decoupling transformation is expressed as a sum of matrices. From the viewpoint of perturbation theory, this scheme is regarded as an application of quasi-degenerate perturbation theory (QDPT) to the relativistic Dirac Hamiltonian. Thus, by using QPDT, we may find more efficient transformations than the Douglas–Kroll transformation.

In this chapter, we propose a formulation of two-component methods based on QPDT. We numerically examine the convergence of the QDPT-based perturbation expansions at lower and higher orders. We also examine the PCE effects of the exactly decoupled one-electron Dirac Hamiltonian by applying the transformation to both one- and many-electron systems.

4.2 Theory

4.2.1 Brief review of conventional two-component methods

In the two-component methods, the one-electron Dirac Hamiltonian is (approximately or exactly) block-diagonalized by a unitary transformation to construct an effective Hamiltonian for the electron part.

$$\mathbf{U}\mathbf{H}\mathbf{U}^{\dagger} = \begin{pmatrix} \mathbf{H}^{+} & \mathbf{0} \\ \mathbf{0} & \mathbf{H}^{-} \end{pmatrix} \tag{4.1}$$

where $\mathbf{H}^{+}$ and $\mathbf{H}^{-}$ are the effective Hamiltonian of positive and negative energy space, respectively. Here, $\mathbf{H}^{+}$ is regarded as the effective Hamiltonian for electrons. Since the decoupling of an operator by a unitary transformation is not unique, there are serval possibilities for the unitary transformation. The Douglas–Kroll (DK) method is one of the most widely known two-component methods. The starting point of the DK method is the free-particle Foldy–Wouthysen transformation $\mathbf{U}^{\mathrm{fpFW}}$, which is defined as a unitary transformation that diagonalizes the free-particle Dirac equation, and is expressed as:

$$\mathbf{U}^{\mathrm{fpFW}} = \begin{pmatrix} \mathbf{A} & \mathbf{A}\mathbf{R} \\ -\mathbf{A}\mathbf{R} & \mathbf{A} \end{pmatrix}, \tag{4.2}$$

whrere **A** and **R** are diagonal matrices. The diagonal elements of these matrices are given by

$$A_i = \left(\frac{E_{0,i} + c^2}{2E_0} \right)_i^{\frac{1}{2}}, \tag{4.3}$$

and

$$R_i = \frac{c\boldsymbol{\sigma}_i \cdot \mathbf{p}_i}{E_{0,i} + c^2} \tag{4.4}$$

with

$$E_{0,i} = \left(p_i^2 c^2 + mc^4\right)^{\frac{1}{2}}. \tag{4.5}$$

Then, transformed Dirac Hamiltonian is thus expressed as:

$$\mathbf{U}^{\mathrm{fpFW}}\mathbf{H}U^{\mathrm{fpFW}} = \mathbf{E}_0 + \mathbf{E}_1 + \mathbf{O}_1 \tag{4.6}$$

with

$$\mathbf{E}_1 = \begin{bmatrix} \mathbf{AVA} + \mathbf{ARVRA} & 0 \\ 0 & \mathbf{AVA} + \mathbf{ARVRA} \end{bmatrix} \tag{4.7}$$

$$\mathbf{O}_1 = \begin{bmatrix} 0 & \mathbf{ARVA} - \mathbf{AVRA} \\ \mathbf{AVRA} - \mathbf{ARVA} & 0 \end{bmatrix} \tag{4.8}$$

where $\mathbf{E}_k$ is the even term, which is block-diagonal, and $\mathbf{O}_k$ is the odd-term, which is block-off-diagonal, and subscript k denotes the order of the term in potential operator $\hat{V}$. Following the Foldy–Wouthysen transformation, multiple unitary transformations are applied in the DK method. The k-th unitary transformation $\mathbf{U}_k$ is expressed as a series of matrix variable $\mathbf{W}_k$:

$$\mathbf{U}_k = \mathbf{1} + \mathbf{W}_k + \frac{1}{2}\mathbf{W}_k^2 + \cdots \tag{4.9}$$

The matrix $\mathbf{W}_k$ is determined so as to cancel the k-th order odd-term $\mathbf{O}_k$. Thus, the matrix $\mathbf{W}_k$ is determined by the equation:

$$[\mathbf{E}_0, \mathbf{W}_i] = -\mathbf{O}_i \tag{4.10}$$

In the conventional DK transformation, successive unitary transformations act as a product resulting in a single unitary transformation:

$$\mathbf{U}^{\mathrm{DK}} = \mathbf{U}^{\mathrm{fpFW}} \prod_{k=1} \mathbf{U}_k. \tag{4.11}$$

The n-th order DK Hamiltonian is determined as LL block of sum of even terms up to the n-th order:

$$\mathbf{H}^{+,\mathrm{DK}n} = \left(\sum_i \mathbf{E}_k\right)^{\mathrm{LL}} \tag{4.12}$$

Another widely known two-component method is the infinite-order two-component (IOTC) method. The starting point of IOTC is the free-particle FW transformation, as in the DK transformation. Following the FW transformation, a single unitary transformation is determined by the block-diagonalizing condition for the Dirac Hamiltonian.

$$\mathbf{U}^{\mathrm{IOTC}} = \mathbf{U}_1\mathbf{U}^{\mathrm{fpFW}} \tag{4.13}$$

$$\mathbf{U}_1 = \frac{1}{\sqrt{1 + \mathbf{Y}^\dagger\mathbf{Y}}}\begin{bmatrix} \mathbf{1} & \mathbf{Y} \\ -\mathbf{Y} & \mathbf{1} \end{bmatrix} \tag{4.14}$$

The matrix $\mathbf{Y}$ is determined so that the off-diagonal block of transformed Hamiltonian is null:

$$(\mathbf{E}_0 + \mathbf{E}_1)\mathbf{Y} + \mathbf{Y}\mathbf{O}_1\mathbf{Y} + \mathbf{O}_1 - \mathbf{Y}(-\mathbf{E}_0 + \mathbf{E}_1). \tag{4.15}$$

This equation (4.14) is not a linear matrix equation, and hence it must be is solved iteratively.

4.2.2 Two-component method based on quasi-degenerate perturbation theory

QDPT is a multi-states perturbation theory, and has been traditionally used in electron correlation problems. In QDPT, the Hamiltonian is partitioned into the zeroth order and perturbation terms, as in the single-state perturbation theory. The eigenfunctions of the zeroth order Hamiltonian are divided into the functions in the model space (P-space) and its complement space (Q-space). The Hamiltonian is then block-diagonalized to obtain and effective Hamiltonian in only the model (P) space:

$$\begin{pmatrix} \mathbf{H}_0^{\mathrm{PP}} + \mathbf{V}^{\mathrm{PP}} & \mathbf{V}^{\mathrm{PQ}} \\ \mathbf{V}^{\mathrm{QP}} & \mathbf{H}_0^{\mathrm{QQ}} + \mathbf{V}^{\mathrm{QQ}} \end{pmatrix} \begin{pmatrix} \mathbf{W}^{\mathrm{PP}} & \mathbf{W}^{\mathrm{PQ}} \\ \mathbf{W}^{\mathrm{QP}} & \mathbf{W}^{\mathrm{QQ}} \end{pmatrix} = \begin{pmatrix} \mathbf{W}^{\mathrm{PP}} & \mathbf{W}^{\mathrm{PQ}} \\ \mathbf{W}^{\mathrm{QP}} & \mathbf{W}^{\mathrm{QQ}} \end{pmatrix} \begin{pmatrix} \mathbf{K}^{\mathrm{PP}} & 0 \\ 0 & \mathbf{K}^{\mathrm{QQ}} \end{pmatrix} \tag{4.16}$$

The transformation matrix *W* is expressed as a sum of matrices. By comparing QP and PP blocks of the both sides of the equation, we obtain the basic equations of QDPT:

$$\begin{cases} \mathbf{K}^{\mathrm{PP}} = \left(\mathbf{H}_0^{\mathrm{PP}} + \mathbf{V}^{\mathrm{PP}}\right)\mathbf{W}^{\mathrm{PP}} + \mathbf{V}^{\mathrm{PQ}}\mathbf{W}^{\mathrm{QP}} - \left(\mathbf{W}^{\mathrm{PP}} - 1\right)\mathbf{K}^{\mathrm{PP}} \\ \left(\mathbf{V}^{\mathrm{PQ}}\right)^{\dagger}\mathbf{W}^{\mathrm{PP}} + \left(\mathbf{H}_{\mathbf{0}}^{\mathrm{QQ}} + \mathbf{V}^{\mathrm{QQ}}\right)\mathbf{W}^{\mathrm{QP}} - \mathbf{W}^{\mathrm{QP}}\mathbf{H}^{\mathrm{PP}} = 0 \end{cases} \tag{4.17}$$

Expanding the effective Hamiltonian $\mathbf{K}^{\mathrm{PP}}$ and the QP and PP parts of the similarity transformation matrix $\mathbf{W}$ by the order of the perturbation:

$$\mathbf{K}^{\mathrm{PP}} = \mathbf{H}_0 + \mathbf{K}_1^{\mathrm{PP}} + \mathbf{K}_2^{\mathrm{PP}} \cdots \tag{4.18}$$

$$\mathbf{W}^{\mathrm{QP}} = \mathbf{W}_1^{\mathrm{QP}} + \mathbf{W}_2^{\mathrm{QP}} \cdots \tag{4.19}$$

$$\mathbf{W}^{\mathrm{PP}} = \mathbf{I} + \mathbf{W}_1^{\mathrm{PP}} + \mathbf{W}_2^{\mathrm{PP}} \cdots \tag{4.20}$$

yields the QDPT working equations:

$$\begin{cases} \left[\mathbf{W}_n^{\mathrm{QP}}, \mathbf{H}_0\right] = -\mathbf{V}^{\mathrm{QP}}\mathbf{W}_{n-1}^{\mathrm{PP}} - \mathbf{V}^{\mathrm{QQ}}\mathbf{W}_{n-1}^{\mathrm{QP}} + \sum_{i=1}^{n-1} \mathbf{W}_i^{\mathrm{QP}}\mathbf{K}_{n-i}^{\mathrm{PP}} \\ \mathbf{K}_n^{\mathrm{PP}} = \mathbf{H}_0^{\mathrm{PP}}\mathbf{W}_n^{\mathrm{PP}} + \mathbf{V}^{\mathrm{PQ}}\mathbf{W}_{n-1}^{\mathrm{QP}} + \mathbf{V}^{\mathrm{PP}}\mathbf{W}_{n-1}^{\mathrm{PP}} - \sum_{i=1}^{n} \mathbf{W}_i^{\mathrm{PP}}\mathbf{K}_{n-i}^{\mathrm{PP}} \end{cases} \tag{4.21}$$

In the two-component method based on QDPT, we partition the one-electron Dirac Hamiltonian into the kinetic operator as the zero-th order Hamiltonian and the potential operator as the perturbation. The space of the electronic solutions is defined as the model space.

Due to the arbitrariness of $\mathbf{W}^{\mathrm{PP}}$, there have been serval versions of QDPT. The condition that removes this arbitrariness is called the normalization condition. In this chapter, three QDPT versions, i.e., the canonical van-Vleck (CVV), Kirtman–Certain–Hirchfelder (KCH), and RS PTs are examined. In CVV-PT, the transformation $\mathbf{W}$ is defined by the exponential of an anti-Hermitian matrix $\mathbf{G}$:

$$\mathbf{W}^{\mathrm{CVV}} = \exp(\mathbf{G}) \tag{4.22}$$

$$\mathbf{G}^{\dagger} = -\mathbf{G}. \tag{4.23}$$

Then, working equation for CVV-PT is rewritten as an equation for $\mathbf{G}$. In KCH-PT, the transformation matrix $\mathbf{W}$ is defined to be unitary. To ensure unitarity of $\mathbf{W}$ at each order, an explicit unitary constrain is imposed:

$$\sum_{i=0}^{n} \mathbf{W}_i^{\mathrm{KCH}} \mathbf{W}_{n-i}^{\mathrm{KCH}} = \mathbf{I}. \tag{4.24}$$

In RS-PT, the diagonal block of transformation $\mathbf{W}^{\mathrm{PP,RS}}$ is set to be unity. Thus, $\mathbf{W}_i^{\mathrm{PP,RS}}$ is zero matrix with excepted for zero-th order:

$$\mathbf{W}_i^{\mathrm{PP,RS}} = \mathbf{0}, i > 0. \tag{4.25}$$

This normalization dose not ensure Hermicity of the effective Hamiltonian. In order to obtain a Hermitian effective Hamiltonian, processing is necessary on the transformation:

$$\mathbf{U}^{\mathrm{Herm}} = \frac{1}{\sqrt{1 + \mathbf{W}^{\mathrm{QP}\dagger}\mathbf{W}^{\mathrm{QP}}}}. \tag{4.26}$$

As a results of this Hermitization, the results of RS-PT coincide with that of the IOTC method at infinite order. Note that it was shown by Shavit and Redmon that the effective Hamiltonians of CVV-PT and Hermitized RS-PT are equivalent at each order[71]. An alternative way of Hermitization is to redefine the effective Hamiltonian by unitary transformation up to the *n*-th order:

$$\mathbf{H}_n^{\mathrm{eff}} = \left(\mathbf{W}^{\dagger}\mathbf{H}^{\mathrm{D}}\mathbf{W}\right)^{\mathrm{LL}} = \left[\left(\sum_{i=0}^{n} \mathbf{W}_i^{\dagger}\right)\mathbf{H}^{\mathrm{D}}\left(\sum_{i=0}^{n} \mathbf{W}_i\right)\right]^{\mathrm{LL}} \tag{4.27}$$

This transformation multiplies the Hamiltonian $\mathbf{H}^{\mathrm{D}}$ by the transformation matrix $\mathbf{W}$ and does not truncate the perturbation order. Therefore, the effective Hamiltonian $\mathbf{H}^{\mathrm{eff}}$ partially includes corrections up to (2*n*+1)-th order. This Hermitization scheme can also be applied to the KCH-PT. Hereafter, we refer to the effective Hamiltonian obtained through this Hermitization as the full-space transformed Hamiltonian.

4.2.3 Picture-change error in two-component method

As stated in Sec. 4.1 (Introduction), PCE is caused by inconsistency of basis and thus is an artificial error in the two-component method. As an example of PCE, consider one-electron properties such as electric dipole moment. The one-electron property is expressed as the trace of a product matrix:

$$\langle \hat{O} \rangle = \mathrm{Tr}(\mathbf{OD}), \tag{4.28}$$

where $\mathbf{O}$ is the matrix representation of operator $\hat{O}$ and $\mathbf{D}$ is the density matrix. It is often the case that in this equation, the density matrix is expressed using the transformed basis set and the matrix $\mathbf{O}$ using only the large component basis set. In such a case, the PCE occurs due to the

mismatch of the basis sets between **O** and **D**. In the case of one-electron properties expressed as Eq. (4.21), the PCE can be corrected by evaluating the operator with the transformed basis set. That is, the PCE corrected expectation value is expressed as

$$\langle \hat{O} \rangle = \mathrm{Tr}\left[\left(\mathbf{U}^{\dagger}\mathbf{O}\mathbf{U} \right)^{\mathrm{LL}} \mathbf{D} \right], \tag{4.29}$$

where **U** is unitary matrix.

The two-electron PCE occurs not only in computing two-electron properties but also in determining wavefunction parameters because the molecular Hamiltonian is a many-electron Hamiltonian and thus contains the two-electron operator. In such cases, the PCE may occur through the two-electron operator. In two-component methods, combination of the one-electron two component Hamiltonian and the non-relativistic two-electron Coulomb operator is commonly used as a many-electron two-component Hamiltonian. However, in this combination, the PCE occurs due to the basis inconsistency between the one- and two-electron operators. More specifically, the one-electron Hamiltonian is expressed in the transformed basis, while the two-electron operator is expressed in the untransformed basis. To avoid this two-electron PCE, the use of the transformed two-electron operator is necessary, and thus it is used in this chapter. The formula of the transformed two-electron integral, which is also called picture-change corrected (PCC) two-electron integral, for two-component method is written as

$$\begin{aligned} (\mu\nu|\lambda\sigma)^{2c} = & W_{\mu p}^{\mathrm{PP}} W_{\nu q}^{\mathrm{PP}} (pq|rs)^{\mathrm{LLLL}} W_{\lambda r}^{\mathrm{PP}} W_{\sigma s}^{\mathrm{PP}} \\ & + W_{\mu p}^{\mathrm{PP}} W_{\nu q}^{\mathrm{PP}} (pq|rs)^{\mathrm{LLSS}} W_{\lambda r}^{\mathrm{QP}} W_{\sigma s}^{\mathrm{QP}} \\ & + W_{\mu p}^{\mathrm{QP}} W_{\nu q}^{\mathrm{QP}} (pq|rs)^{\mathrm{SSLL}} W_{\lambda r}^{\mathrm{PP}} W_{\sigma s}^{\mathrm{PP}} \\ & + W_{\mu p}^{\mathrm{QP}} W_{\nu q}^{\mathrm{QP}} (pq|rs)^{\mathrm{SSSS}} W_{\lambda r}^{\mathrm{QP}} W_{\sigma s}^{\mathrm{QP}} \end{aligned} \tag{4.30}$$

with

$$(pq|rs)^{XXYY} = \int d\mathbf{r}_1 d\mathbf{r}_2 \, \chi_p^X(\mathbf{r}_1) \chi_q^X(\mathbf{r}_1) \frac{1}{|\mathbf{r}_1 - \mathbf{r}_2|} \chi_r^Y(\mathbf{r}_2) \chi_s^Y(\mathbf{r}_2) \tag{4.31}$$

and

$$\chi_p^{\mathrm{S}}(\mathbf{r}_1) = \frac{\boldsymbol{\sigma} \cdot \hat{\mathbf{p}}}{2c} \chi_p^{\mathrm{L}}(\mathbf{r}_1), \tag{4.32}$$

where **W** is the transformation matrix dependent on the two-component methods and $(pq|rs)^{XXYY}$ are two-electron integrals in large and small component basis sets in the Muliken notation. χ_p^{L} and χ_p^{S} are the large- and small-component basis functions. The kinetic balance is employed for the small-component basis functions. The explicit formulas of the two-electron integrals were reported in the BP, IOTC[72], NESC[73], and up to third order DK[74][75][64] methods. Though the two-electron operator is desired to be consistent with one-electron Hamiltonian at each order, we do not employ such a two-electron operator, but the operator multiplied by the sum of the matrices up to the *n*-th order **W**.

$$\mathbf{W} = \sum_{i=0}^{n} \mathbf{W}_i \tag{4.33}$$

In this case, the two-electron term operator partially includes the higher order corrections. The maximum order included is 2n+1.

We now consider picture-change corrected single reference methods. First, consider the picture-change corrected Hartree–Fock method, which is a starting point of single reference methods. The Fock matrix is the sum of the one-electron core-Hamiltonian matrix and the two-electron Fock part, namely, the sum of the Coulomb and exchange matrices:

$$\mathbf{F} = \mathbf{H}^{+} + \mathbf{G}^{2c} \tag{4.34}$$

with

$$\mathbf{G}^{2c} = \mathbf{J}^{2c} - \mathbf{K}^{2c} \tag{4.35}$$

$$J_{\mu\nu}^{2c} = D_{\sigma\lambda}(\mu\nu|\lambda\sigma)^{2c} \tag{4.36}$$

$$K_{\mu\nu}^{2c} = D_{\sigma\lambda}(\mu\sigma|\lambda\nu)^{2c}. \tag{4.37}$$

This formula is formally identical to the nonrelativistic Fock matrix but is different molecular integrals. The electron correlation methods such as MP2 or CCSD can be performed in the same procedure as the usual non-PCC correlation methods, using the PCC two-electron integrals. In the MP2 case, correlation energy is given using the PC-corrected two-electron integrals and orbital energies ϵ as

$$E_{\mathrm{corr}}^{\mathrm{MP2}} = \frac{1}{4}\sum_{ijab} \frac{[(ia|jb)^{2c} - (ib|ja)^{2c}]^2}{\epsilon_i + \epsilon_j - \epsilon_a - \epsilon_b} \tag{4.38}$$

where the orbitals and their energies are determined by the PCC-HF equation. The PC-corrected coupled-cluster theories is also obtained by replacing the two-electron integrals in the correlation energy and the amplitude equations.

4.3 Results and discussion

To examine the accuracy of the two-component method based on the quasi-degenerate perturbation theory, we performed numerical calculations on several systems: the hydrogen-like atom (Z=80) and radon atom.

4.3.1 One-electron system: hydrogen-like atom with Z=80

In perturbation theory, both convergence of energy spectra at higher and infinite orders and accuracy when truncated at lower orders are important. As a first test system, we examined the convergence property and accuracy using a one-electron system, which does not include a two-electron operator, namely, the hydrogen-like atom with Z=80. The basis set used was an even-tempered s-type gaussian functions with their exponents given by $\{\zeta = \exp(-4.56 +$

$0.72n), n = 1,2, \ldots 50\}$. CVV-, KCH-, and RS-PT were examined using the original and full-space transformed Hamiltonians.

Figure 1 shows the energy differences of the CVV, KCH, RS, KCH(FT), and RS(FT) energies from the IOTC energy, where FT denotes full-space transformation. Note that the IOTC energy is identical to that of the infinite order perturbation theory. For one-electron systems, the exact decoupled Hamiltonian such as the IOTC Hamiltonian is available, which gives identical energy to that of the Dirac equation. As seen from Fig. 4.1, all QDPT versions show no energy divergence and converge smoothly to the IOTC energy. The convergence behavior differs significantly between the full-space transformed Hamiltonian and the original QDPTs. The full-space transformed Hamiltonian QDPTs converge faster than the original QDPTs at all perturbation orders. This results from the inclusion of higher-order corrections in the full-space transformed Hamiltonian. The two full-space transformed Hamiltonian QDPTs show very similar behavior between KCH-PT and RS-PT. In the original QDPTs, KCH-PT shows slightly smaller errors at all perturbation orders than RS-PT and CVV-PT. RS-PT and CVV-PT give almost identical values. Based on these results, KCH-PT and RS-PT will be used in the subsequent discussion.

Then, compare the accuracies of the QDPTs at lowest several (up to the 5th) orders. Table 4.1 shows the energy difference from IOTC up to the 5th order. The original QDPT energies oscillate positively and negatively in error from the IOTC energy, while the errors in the full-space transformed Hamiltonian QDPT are always negative. The errors of the second-order energies of the full-space Hamiltonian QDPT are −0.282068 and −0.353861 a.u. for KCH- and RS-PT, respectively, which roughly correspond to the errors of the 5th order values of the conventional QDPT (−0.261182 and − 0.610218 a.u. for KCH- and RS-PT, respectively). These results are consistent with the fact that the full-space Hamiltonian QDPT partially includes corrections up to the (2*n*+1) order.

For one-electron systems, the energy values given by exact decoupling of the Dirac Hamiltonian are necessarily identical regardless of the two-component methods. However, molecular properties are generally dependent on the two-component methods due to the picture change effects (PCE). To examine the PCE of various two-component methods, we calculated the expected values of r^2 and r^{-1} and their picture change corrections. The results are shown in Table 4.2. Values calculated conventional two-component methods (DK, IOTC, and X2C) and the Dirac Hamiltonian diagonalization method, , as well as the exact values by the Dirac equation (DEQ), are also shown in the table 4.2. All the two-component methods give the same energy value as DEQ, but different expectation values of r^2 and r^{-1} from DEQ when PCE is uncorrected. The Dirac Hamiltonian diagonalization method with large PCE shows very large error for $\langle r^2 \rangle$ and $\langle r^{-1} \rangle$. All the other two-components methods give close values each other

($\langle r^2 \rangle$ =3.3839119, 3.3837647, and 3.4015151 a. u. for KCH, RS, and X2C, respectively and $\langle r^{-1} \rangle$ = 1.1119670, 1.1127953, and 1.1016912 for KCH, RS, and X2C, respectively). Expectation values of KCH-PT are close to the expectation values of DK(3.3839118 and 1.1119687 for $\langle r^2 \rangle$ and $\langle r^{-1} \rangle$, respectively) , while RS-PT gives the same values as the IOTC value, namely: 3.3837647 and 1.1127953 for $\langle r^2 \rangle$ and $\langle r^{-1} \rangle$, respectively. X2C gives different values from either RS or KCH. These results come from the fact that the Hermitized RS transformation matrix is same as that of IOTC and that KCH is equivalent to the DK method of Peng and Hirao. The picture-change corrected expectation values in the table naturally all agree with the DEQ value, including the Dirac Hamiltonian diagonalization method.

4.3.2 Many-electron system: radon atom

In many-electron systems, total energy does not agree with that of the four-component method even using the transformation matrix block-diagonalizing the one-electron Dirac Hamiltonian due to the two-electron PCE. Thus, the converged values are not identical to the values of four-component method and depend on the QDPT versions.

To examine the convergence behavior for many electron systems, we performed Hartree–Fock calculations for the radon atom with and without the picture-change correction. The basis set used was Dyall's triple zeta basis set. The results are shown in Fig. 4.2.

All QDPTs with and without the picture-change correction give converged energies. The convergence behaviors of original QDPTs are similar to the case of the one-electron system. In full-space transformed Hamiltonian QDPT, the errors are always smaller than the original QDPTs at each order as in the one-electron system case. However, the convergence speed is not as fast as the one-electron system case. For the one-electron system, the difference in normalization (i.e., the difference in QDPT version) little affected to total energy in the case of full-space transformed Hamiltonian method. In contrast, for the many-electron system, the differences in normalization are pronounced, especially when using the PCC two-electron operator. KCH-PT converges oscillatively and RS-PT n converges monotonically. These are the opposite of the original QDPTs, where KCH converges monotonically and RS converges oscillatively. In Fig. 4.3, the convergence behaviors of one- and two-electron energies in the total energy are shown. The original QDPT graphs in Figs. 4.3(a) and 4.3(b) indicate that the error in one-electron energy is two digits larger than the error in two-electron energy. Thus, the one-electron energy error is dominant in the total error. On the other hand, the graphs of the full-space transformed Hamiltonian QDPTs in Figs. 4.3(c) and 4.3(d) indicate that the errors in two-electron energy are not as small as the original QDPTs. The full-space transformed RS-PT shows interesting results that differ from the others: at lower orders, the slope of the graph is close to that of the one-electron system, but at higher orders, the slope becomes more gentle

than at lower orders.

Then, we performed electron correlation calculations, namely, the second-order Møller–Plesset (MP2) and coupled cluster singles and doubles (CCSD) calculations using the same basis set as the HF calculations. The convergence behaviors of the correlation energy are shown in Fig. 4.4. The errors in correlation energy are small because the correlation energy is generally smaller than the HF energy. The convergence behavior of the conventional QDPTs without using the PCC two-electron operator are similar to that of the HF energy in Fig. 4.3. The convergence of the full-space transformed Hamiltonian QDPTs is faster than the conventional QDPTs. The converged energy values are shown in Table 4.3. In the picture-change uncorrected Dirac Hamiltonian diagonalization method, SCF had not converged. The combination with the nonrelativistic two-electron operator gives different converged values, while the combination with the picture-change corrected tow-electron operator gives same converged values, namely: –23574.0913, –3.136497, and –2.902747 a. u. for Hartree-Fock energy, MP2 and CCSD correlation energy. In combination with nonrelativistic two-electron operator, the error form two-electron PCE at infinity order in the HF energy are 10.667, 10.9019, and 9.6501 a. u. for KCH-PT, RS-PT, and X2C, respectively. The magnitude of two-electron PCE was almost independent on the QDPT versions. For the correlation energy, the QDPT versions also little affect magnitude of two-electron PCE. The picture-change corrected methods give identical correlation energy. When nonrelativistic two-electron integrals are employed, the converged values depend on the QDPT versions. In contrast, the picture-change corrected methods give the values that were identical to each other and almost identical to the four-component correlation energy. The energy derivation from four-component method arise unitary transformation determined by one-electron Dirac Hamiltonian. In two-component methods based on QDPT, the normalization little affect the correlation energy rather than two-electron PCE.

Expectation value of r^2 and r^{-1} at infinity order using Hartree–Fock wavefunction are shown in table 4.3. The expectation values of r^2 and r^{-1} are the quantities that mainly reflect electron densities in the far from the nuclear and near the nuclear, respectively. In molecular property, there are two sources of PCE, namely: determination of wavefunction and property operator. In PC-uncorrected property, PCC Dirac Hamiltonian diagonalization method give far form values(58.37039 and 90368.05849 a. u. for $\langle r \rangle$ and $\langle r \rangle$, respectively) other two-component methods. For the expectation value of r^2, PC-uncorrected values are about 76.21 and 76.18 a. u. for two-electron PC-uncorrected or -corrected method. PCE from property operator was 0.002 a. u.. In this case, two-electron PCE form determination wavefunction is larger than PCE from property operator. In contrast, for the expectation value of r^{-1}, PCE from property operator is main source of PCE.

The errors in HF, MP2, CCSD energies are shown in Tables 4.4–4.6. At the lowest several,

orders, the errors originate from PC and incomplete block diagonalization. In the Hartree–Fock method, the error coming from the PC is around 10 Hartree, while in the correlated methods, the errors in correlation energy mainly come from the PC even at the second order, and the increasing perturbation order dose not improved accuracy so much.

4.4 Conclusion

In Chapter 4, we formulated the two-component method based on QDPT. Both the convergence of energy spectra at higher and infinite orders and accuracy when truncated at lower orders were discussed. For the one-electron system, all QDPTs converge smoothly to the IOTC energy with no energy divergence. The convergence behavior differed significantly between the full-space transformed Hamiltonian and original QDPTs. The full-space transformed Hamiltonian QDPTs converge faster than the original QDPTs at all perturbation orders. This results from the partial inclusion of higher-order corrections in the full-space transformed Hamiltonian. In the original QDPTs, KCH-PT showed slightly smaller errors than RS-PT and CVV-PT at all perturbation orders. RS-PT and CVV-PT gave almost identical values. For the converged values of expectation value of r^2 and r^{-1}, the PC-uncorrected exception values depended on two-component methods. The Dirac Hamiltonian diagonalizing method showed large PCE. In contrast, the PC-corrected exception values were identical in all the two-component method including the diagonalizing method.

In the many-electron radon atom, all QDPTs converged both with and without PC-corrected two-electron operator. The convergence behavior of the full-space transformed Hamiltonian QDPT differed from that of the one-electron system because the errors in two-electron energy were not small enough to neglect compared with those in one-electron energy. Although the convergence speed was not faster than the one-electron system, the full-space transformed Hamiltonian QDPT gave smaller error than the original QDPTs. In PC-uncorrected method, the converged values depended on the two-component methods were not identical due to the two-electron PCE. In contrast, the PC-corrected methods gave identical values for not only one-electron properties, Hartree–Fock energy, and MP2 correlation energy dependent on only the one-electron density matrix, but also for the CCSD correlation energy dependent on the two-electron density matrix.

Table 4.1 Energy difference from IOTC energy (−3532.192128 a.u.) up to the 5th order.

Perturbation order	KCH	RS	KCH(FT)	RS(FT)
2	8.867242	9.050460	−0.282068	−0.353861
3	−0.927488	−5.091089	−0.036225	−0.049806
4	0.483514	0.878599	−0.008365	−0.011130
5	−0.261182	−0.610218	−0.001840	−0.002401

Table 4.2 1s orbital energy and exception values of $\boldsymbol{r^2}$ and $\boldsymbol{r^{-1}}$ (**in a**. **u**.).

	Energy	$\langle r^2 \rangle \times 10^{-4}$	$\langle \mathbf{U}^\dagger r^2 \mathbf{U} \rangle \times 10^{-4}$	$\langle r^{-1} \rangle \times 10^{2}$	$\langle \mathbf{U}^\dagger r^{-1} \mathbf{U} \rangle \times 10^{2}$
KCH	−3532.192128	3.3839119	3.7141427	1.1119670	0.9853358
RS	−3532.192128	3.3837647	3.7141427	1.1127953	0.9853358
X2C	−3532.192128	3.4015151	3.7141427	1.1016912	0.9853358
Diagonalizing	−3532.192128	744299.6572006	3.7141427	0.0013065	0.9853358
DK35(EXP)	−3532.192128	3.3839118		1.1119687	
IOTC	−3532.192128	3.3837647		1.1127953	
DEQ	−3532.192128	3.7141427		0.9853358	

Table 4.3 Hartree–Fock and correlation (MP2 and CCSD) energies for the radon atom obtained from the exact decoupling transformation of Dirac Hamiltonian (in a.u.)

	HF	MP2	CCSD
picture-change uncorrected			
KCH	–23563.3914	–3.2055394	–2.9715317
RS	–23563.3782	–3.2055925	–2.9715850
X2C	–23564.4300	–3.2040225	–2.9700177
Diagonalizing	not converge	NA	NA
picture-change corrected			
KCH	–23574.0913	–3.136497	–2.902747
RS	–23574.0913	–3.136497	–2.902747
X2C	–23574.0913	–3.136497	–2.902747
Diagonalizing	–23574.0913	–3.136497	–2.902747
Four-Component	−23574.0801	−3.136543	−2.902765

Table 4.4 Converged value of properties $\boldsymbol{r^2}$ and $\boldsymbol{r^{-1}}$ for the radon atom (in a.u.)

	$\langle r^2 \rangle$	$\langle \mathbf{U}^\dagger r^2 \mathbf{U} \rangle$	$\langle r^{-1} \rangle$	$\langle \mathbf{U}^\dagger r^{-1} \mathbf{U} \rangle$
KCH/NR	76.216958	76.214950	734.307860	696.396205
RS/NR	76.216971	76.214962	734.604309	696.395416
X2C/NR	76.21334	76.21130	731.77369	696.43990
KCH/KCH	76.186359	76.184350	734.858977	696.865769
RS/RS	76.186359	76.184350	735.157071	696.865769
X2C/X2C	76.186385	76.184350	732.273350	696.865769
Diag /Diag	58.37039	76.184350	90368.05849	696.865769

Table 4.5 Energy deviation from the four-component Hartree–Fock energy (−23574.08005 a.u.) for the radon atom

	No two-electron PCC				Two-electron PCC			
	KCH	RS	KCH(FT)	RS(FT)	KCH	RS	KCH(FT)	RS(FT)
2	40.7703	41.4431	9.6105	9.3274	29.9989	30.8213	−1.2216	-1.3563
3	7.3782	−8.5812	10.5456	10.5111	−3.1794	−19.3266	−0.0057	−0.1951
4	12.4704	14.0281	10.6598	10.6632	1.7583	3.3253	−0.0560	−0.0463
5	9.6778	8.1996	10.6827	10.6943	−1.0039	−2.5174	0.0030	−0.0175

Table 4.6 Energy derivation from four-component MP2 correlation energy (–3.136542918 a.u.) for radon atom.

	No two-electron PCC				Two-electron PCC			
	KCH	RS	KCH(FT)	RS(FT)	KCH	RS	KCH(FT)	RS(FT)
2	−0.06842	−0.06840	−0.06907	−0.06908	0.00038	0.00033	0.00000	−0.00006
3	−0.06909	−0.06950	−0.06900	−0.06905	−0.00010	−0.00024	−0.00004	0.00003
4	−0.06896	−0.06898	−0.06900	−0.06905	0.00007	0.00008	0.00004	0.00004
5	−0.06902	−0.06911	−0.06900	−0.06905	0.00002	0.00001	0.00003	0.00004

Table 4.7 Energy derivation from four-component CCSD correlation energy (−2.902765141 a.u.) for the radon atom

	KCH	RS	KCH(FT)	RS(FT)	KCH	RS	KCH(FT)	RS(FT)
2	−0.068319	−0.068307	-0.068837	−0.068842	0.000223	0.000171	−0.000021	−0.000082
3	−0.068837	−0.069188	-0.068767	−0.068818	−0.000109	−0.000180	−0.000068	0.000000
4	−0.068738	−0.068761	-0.068771	−0.068820	0.000031	0.000035	0.000015	0.000007
5	−0.068785	−0.068866	-0.068766	−0.068819	−0.000003	−0.000007	0.000006	0.000015

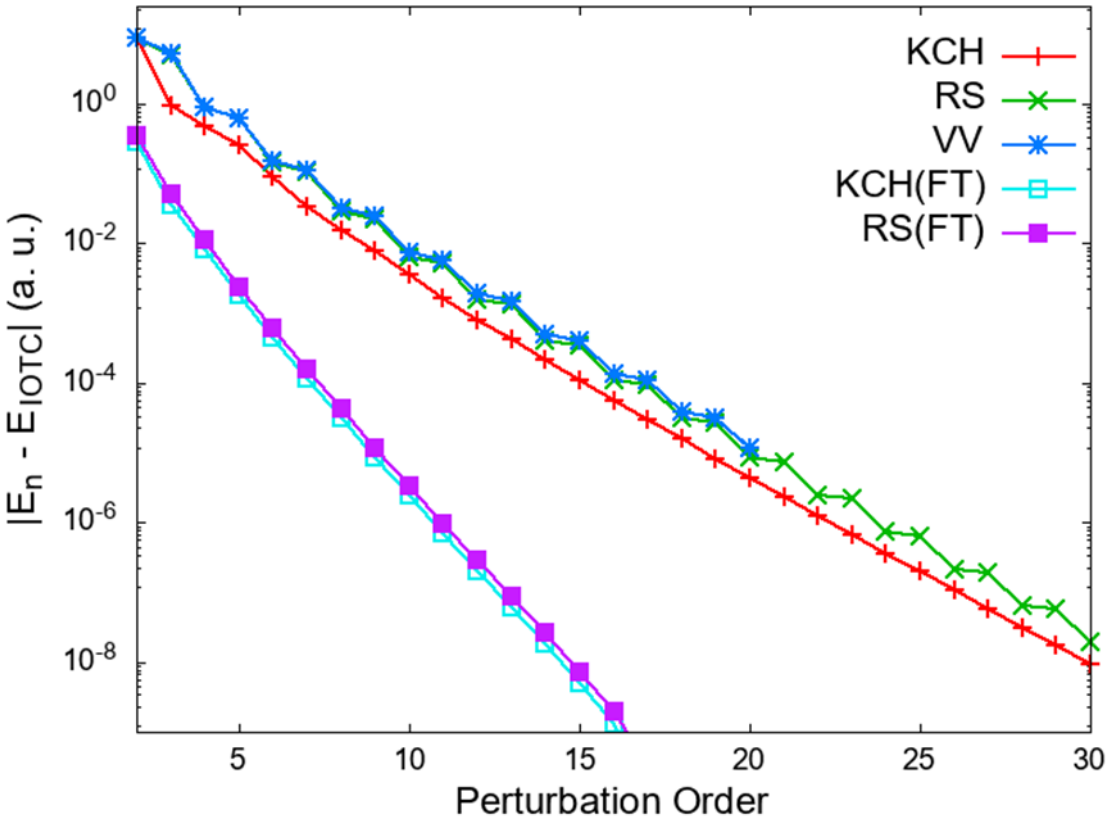

Figure 4.1 Convergence of 1s orbital energy of the hydrogen-like atom (Z=80).

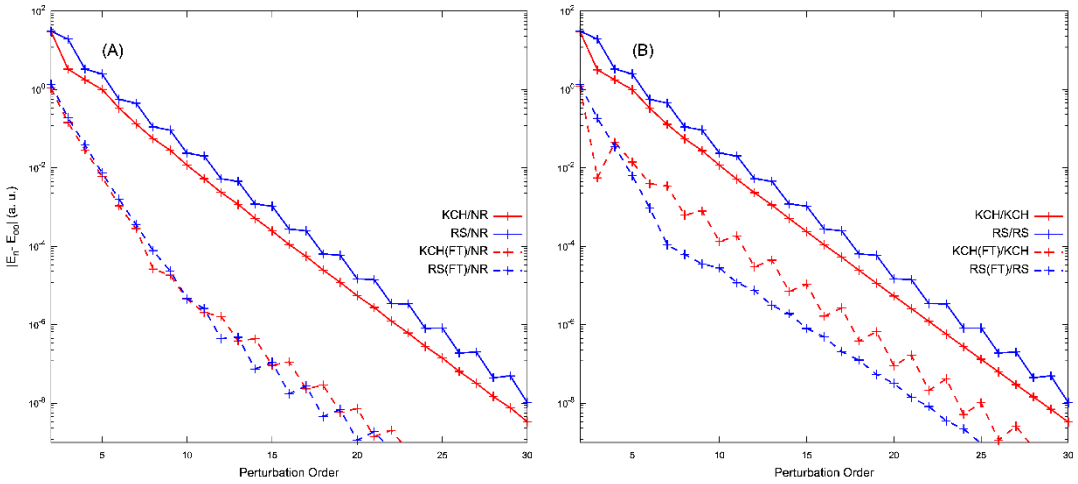

Figure 4.2 Convergence of SCF energy of radon atom (A) without two-electron picture-change correction and (B) with two-electron picture-change correction

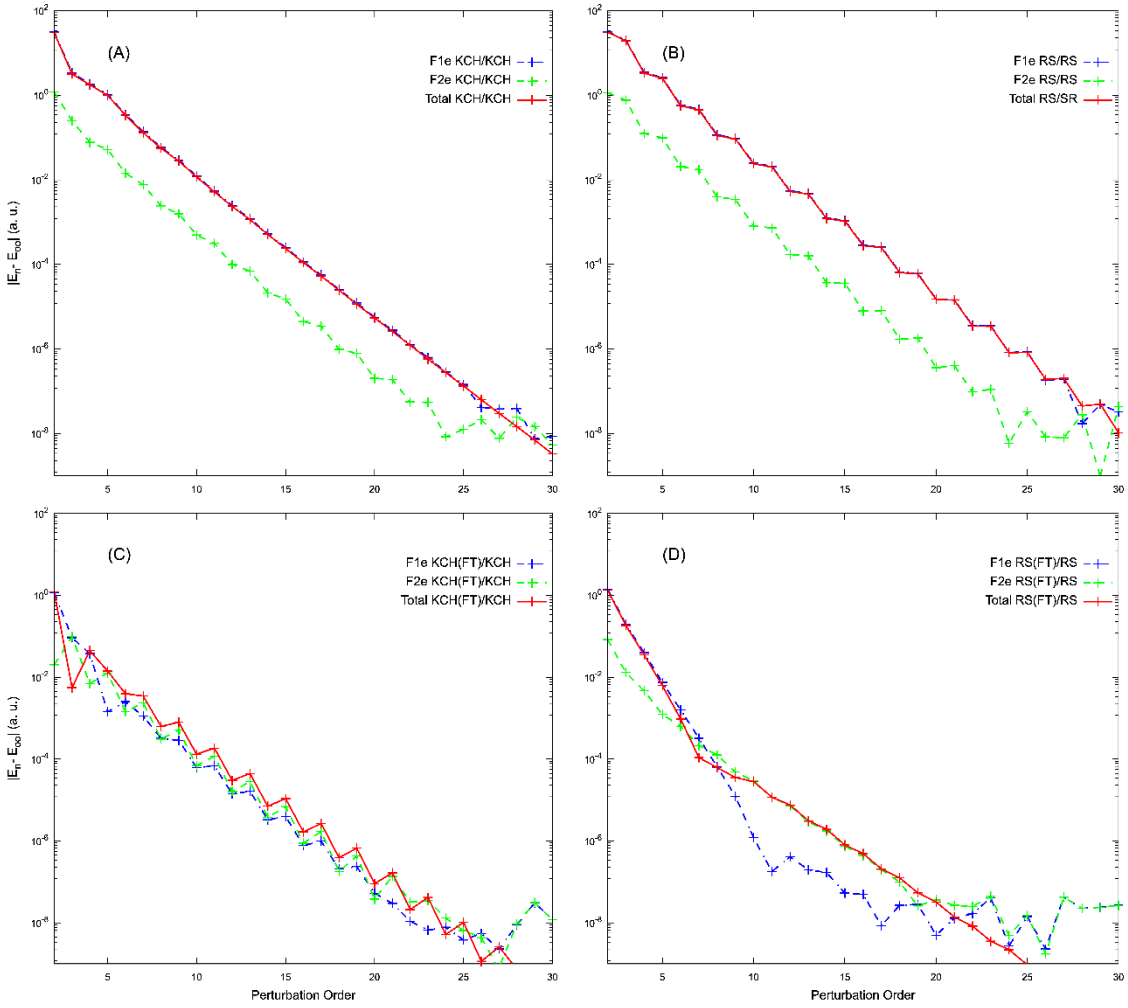

Figure 4.3 Convergence of one- and two-electron energies for (A)KCH/KCH, (B) RS/RS, (C)KCH(FT)/KCH, and (D)RS(FT)/RS

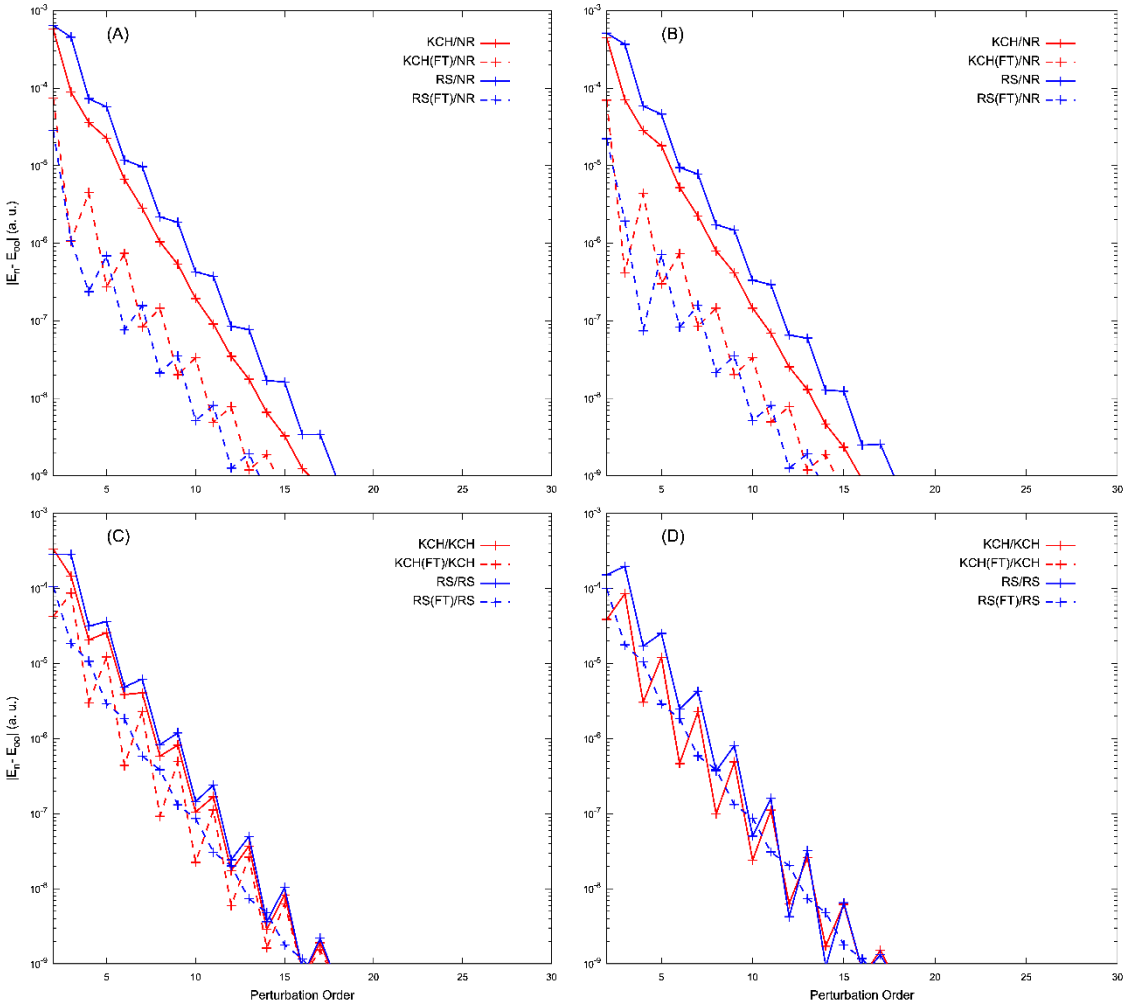

Figure 4.4 Convergence of correlation energy (A) MP2 with uncorrected-PCE two-electron integral (B) CCSD with uncorrected-PCE two-electron integral (C) MP2 with PCC two-electron integral (D) CCSD with PCC two-electron integral

Chapter 5.

General conclusions

In this thesis, relativistic electronic structure theories for solvated molecules have been presented. In Chapter 2, we proposed the hybrid method of DHF and RISM. This method was formulated as a variational problem of the Helmholtz energy, and the analytic energy gradients were also derived using the variational property. We applied the DHF/RISM-SCF method to various systems in aqueous solutions: iodine ion I^-, methyl iodide CH_3I, and hydrogen chalcogenide H_2X. For I^- and CH_3I, the SFEs and their components, and the RDFs of solvent around the I atoms were shown and discussed. DHF/RISM-SCF give reasonable results for these in term of the nature of the compounds. The relativistic effects on solvation structure for CH_3I were relatively small. In contrast, for the electronic structures of solute molecule, the relativistic description using the DHF/RISM-SCF method was essential. For H_2X, the molecular structures, SFE and their components, the electric dipole moment and ESP charges of the solute, and the RDF of solvent around the X and H atoms were computed and discussed focusing mainly on the differences due to the heavy atom X. As shown by the dipole moment results, the polarity of molecule decreased with increasing chalcogen atomic number. DHF/RISM-SCF gives results consistent with molecular polarity in both SEF and RDF.

In Chapter 3, we have applied the DHF/RISM-SCF method to a chemical reaction We made Helmholtz energy profiles of a Menshutkin reaction $NH_3 + CH_3I \rightarrow NH_3CH_3^+ + I^-$ and conducted component analysis. The reaction profile by the RISM-SCF method well described the characteristics of the Menshutkin reaction, and the component analysis revealed the contributions of the effects of electron reorganization and electrostatic and non-electrostatic interactions.

In Chapter 4, we have proposed a new two-component method based on QDPT. Both convergence of energy spectra at higher and infinite orders and accuracy when truncated at lower orders, expectation values were discussed. We applied the method to hydrogen like atom with Z=80 and the radon atom. All two-component methods based on QDPT converged in both one- and many-electron systems. Full-space transformed Hamiltonian show faster convergence than its original QDPTs both one- and many-electron systems. The convergence behavior of the full-space transformed Hamiltonian QDPTs in many-electron system differed from the one-electron system. In the full-space transformed Hamiltonian QDPTs, the errors in two-electron energy were not as small as the errors in one-electron energy. Although the convergence was not faster than the one-electron system, the full-space transformed Hamiltonian QDPT gave smaller

error than the original QDPTs. In PC-uncorrected method, the converged values depended on the two-component method and were not identical due to the two-electron PCE. On the other hand, the PC-corrected methods gave identical values not only one-electron properties, Hartree-Fock energy, and MP2 correlation energy which are related only one-electron density matrix but also CCSD correlation energy which depends on two-electron density matrix.

The method developed this thesis allow us more precious description of solvated heavy element containing molecules used in various field. For further development for theoretical treatment of such molecules, two issues need to be resolved: including electron correlation effects to four-component RISM-SCF and solvent effects to picture-change corrected electronic structure theory. The former is necessary for quantitative description of chemical reaction and molecular properties and can be solved by extension of the method developed by chapter 2 and 3. The latter is necessary for development of less computational demanding method and extension to the method developed by chapter 4.

Bibliography

[1] W. Greiner, “Relativistic Quantum Mechanics. Wave Equations”, Springer Berlin Heidelberg, Berlin, Heidelberg (2000).

[2] B. Bertha Swirles, *Proc. R. Soc. London. Ser. A - Math. Phys. Sci.*, **152**, 625–649 (1935).

[3] I.P. Grant, *Proc. R. Soc. London. Ser. A. Math. Phys. Sci.*, **262**, 555–576 (1961).

[4] G. Malli and J. Oreg, *J. Chem. Phys.*, **63**, 830–841 (1975).

[5] L. Visscher, O. Visser, P.J.C. Aerts, H. Merenga, and W.C. Nieuwpoort, *Comput. Phys. Commun.*, **81**, 120–144 (1994).

[6] E. Engel and R.M. Dreizler, *Density Funct. Theory II*, 1–80 (1996).

[7] L. Belpassi, L. Storchi, H.M. Quiney, and F. Tarantelli, *Phys. Chem. Chem. Phys.*, **13**, 12368 (2011).

[8] W.R. Johnson, M. Idrees, and J. Sapirstein, *Phys. Rev. A*, **35**, 3218 (1987).

[9] Y. Ishikawa, *Phys. Rev. A*, **42**, 1142 (1990).

[10] K.G. Dyall, *Chem. Phys. Lett.*, **224**, (1994).

[11] L. Visscher, T. Saue, W.C. Nieuwpoort, K. Faegri, and O. Gropen, *J. Chem. Phys.*, **99**, 6704–6715 (1993).

[12] Y. Watanabe and O. Matsuoka, *J. Chem. Phys.*, **116**, 9585–9590 (2002).

[13] L. Visscher, T.J. Lee, and K.G. Dyall, *J. Chem. Phys.*, **105**, 8769–8776 (1996).

[14] O. Matsuoka, N. Suzuki, T. Aoyama, and G. Malli, *J. Chem. Phys.*, **73**, 1320–1328 (1980).

[15] H. Jo/rgen Aa. Jensen, K.G. Dyall, T. Saue, and K. Fægri, *J. Chem. Phys.*, **104**, 4083–4097 (1996).

[16] T. Fleig, J. Olsen, and L. Visscher, *J. Chem. Phys.*, **119**, 2963–2971 (2003).

[17] Y. Ishikawa, M.J. Vilkas, and K. Koc, *Int. J. Quantum Chem.*, **77**, 433–445 (2000).

[18] M. Miyajima, Y. Watanabe, and H. Nakano, *J. Chem. Phys.*, (2006).

[19] M. Abe, T. Nakajima, and K. Hirao, *J. Chem. Phys.*, **125**, 234110 (2006).

[20] T. Fleig, L.K. Sørensen, and J. Olsen, *Theor. Chem. Acc.*, **118**, 347–356 (2007).

[21] R.J. Anderson and G.H. Booth, *J. Chem. Phys.*, **153**, (2020).

[22] S. Knecht, Ö. Legeza, and M. Reiher, *J. Chem. Phys.*, **140**, (2014).

[23] R. Di Remigio, R. Bast, L. Frediani, and T. Saue, *J. Phys. Chem. A*, **119**, 5061–5077 (2015).

[24] E. Cancès, B. Mennucci, and J. Tomasi, *J. Chem. Phys.*, **107**, 3032–3041 (1997).

[25] R. Di Remigio, M. Repisky, S. Komorovsky, P. Hrobarik, L. Frediani, and K. Ruud, *Mol. Phys.*, **115**, 214–227 (2017).

[26] E.D. Hedegård, R. Bast, J. Kongsted, J.M.H. Olsen, and H.J.A. Jensen, *J. Chem. Theory*

Comput., **13**, 2870–2880 (2017).

[27] D. Chandler, *J. Chem. Phys.*, **57**, 1930 (1972).

[28] F. Hirata, "Molecular Theory of Solvation", Ed. by F. Hirata, Kluwer Academic Publishers, Dordrecht (2004).

[29] S. Ten-no, F. Hirata, and S. Kato, *Chem. Phys. Lett.*, **214**, 391–396 (1993).

[30] S. Ten-No, F. Hirata, and S. Kato, *J. Chem. Phys.*, **100**, 7443–7453 (1994).

[31] H. Sato, F. Hirata, and S. Kato, *J. Chem. Phys.*, **105**, 1546–1551 (1996).

[32] N. Yoshida, *Condens. Matter Phys.*, **10**, 363–372 (2007).

[33] F.A. Momany, *J. Phys. Chem.*, **82**, 592–601 (1978).

[34] S.R. Cox and D.E. Williams, *J. Comput. Chem.*, **2**, 304–323 (1981).

[35] T.H. Dunning, *J. Chem. Phys.*, **90**, 1007–1023 (1989).

[36] D.E. Woon and T.H. Dunning, *J. Chem. Phys.*, **98**, 1358–1371 (1993).

[37] K.G. Dyall, *Theor. Chem. Acc.*, **115**, 441–447 (2006).

[38] A.K. Rappé, C.J. Casewit, K.S. Colwell, W.A. Goddard, and W.M. Skiff, *J. Am. Chem. Soc.*, **114**, 10024–10035 (1992).

[39] Y. Sakiyama, S. Takagi, and Y. Matsumoto, *J. Chem. Phys.*, **122**, (2005).

[40] H.J.C. Berendsen, J.R. Grigera, and T.P. Straatsma, *J. Phys. Chem.*, **91**, 6269–6271 (1987).

[41] M.D. Cookson and P.M.R. Stirk, (2019).

[42] T. Saue, R. Bast, A.S.P. Gomes, H.J.A. Jensen, L. Visscher, I.A. Aucar, R. Di Remigio, K.G. Dyall, E. Eliav, E. Fasshauer, T. Fleig, L. Halbert, E.D. Hedegård, B. Helmich-Paris, M. Iliaš, C.R. Jacob, S. Knecht, J.K. Laerdahl, M.L. Vidal, et al., *J. Chem. Phys.*, **152**, 204104 (2020).

[43] D. Chandler and H.C. Andersen, *J. Chem. Phys.*, **57**, 1930–1937 (1972).

[44] N. Yoshida and F. Hirata, *J. Comput. Chem.*, **27**, 453–62 (2006).

[45] D. Beglov and B. Roux, *J. Phys. Chem. B*, **101**, 7821–7826 (1997).

[46] A. Kovalenko and F. Hirata, *Chem. Phys. Lett.*, **290**, 237–244 (1998).

[47] L. Blum and A.J. Torruella, *J. Chem. Phys.*, **56**, 303–310 (1972).

[48] L. Blum, *J. Chem. Phys.*, **58**, 3295–3303 (1973).

[49] A. Kovalenko and F. Hirata, *J. Chem. Phys.*, **110**, 10095–10112 (1999).

[50] H. Sato, A. Kovalenko, and F. Hirata, *J. Chem. Phys.*, **112**, 9463–9468 (2000).

[51] N. Yoshida and S. Kato, *J. Chem. Phys.*, **113**, 4974–4984 (2000).

[52] K.G. Dyall and K. Faegri, "Introduction to Relativistic Quantum Chemistry", Oxford University Press, New York (2007).

[53] J. Tomasi, B. Mennucci, and R. Cammi, *Chem. Rev.*, **105**, 2999–3093 (2005).

[54] M. Cossi, N. Rega, G. Scalmani, and V. Barone, *J. Comput. Chem.*, **24**, 669–681 (2003).

[55] A. V. Marenich, C.J. Cramer, and D.G. Truhlar, *J. Phys. Chem. B*, **113**, 6378–6396 (2009).
[56] K. Okamoto, S. Fukui, and H. Shingu, *Bull. Chem. Soc. Jpn.*, **40**, 1920–1925 (1967).
[57] K. Okamoto, S. Fukui, I. Nitta, and H. Shingu, *Bull. Chem. Soc. Jpn.*, **40**, 2354–2357 (1967).
[58] R. van Leeuwen, E. van Lenthe, E.J. Baerends, and J.G. Snijders, *J. Chem. Phys.*, **101**, 1272–1281 (1994).
[59] K.G. Dyall and E. Van Lenthe, *J. Chem. Phys.*, **111**, 1366–1372 (1999).
[60] T. Nakajima and K. Hirao, *Chem. Phys. Lett.*, **302**, 383–391 (1999).
[61] M. Douglas and N.M. Kroll, *Ann. Phys. (N. Y).*, **82**, 89–155 (1974).
[62] B.A. Hess, *Phys. Rev. A*, **32**, 756–763 (1985).
[63] B.A. Hess, *Phys. Rev. A*, **33**, 3742–3748 (1986).
[64] T. Nakajima and K. Hirao, *J. Chem. Phys.*, **119**, 4105–4111 (2003).
[65] A. Wolf, M. Reiher, and B.A. Hess, *J. Chem. Phys.*, **117**, 9215–9226 (2002).
[66] C. Van Wüllen, *J. Chem. Phys.*, **120**, 7307–7313 (2004).
[67] M. Barysz and A.J. Sadlej, *J. Chem. Phys.*, **116**, 2696–2704 (2002).
[68] W. Kutzelnigg and W. Liu, *J. Chem. Phys.*, **123**, (2005).
[69] M. Iliaš and T. Saue, *J. Chem. Phys.*, **126**, (2007).
[70] D. Peng and K. Hirao, *J. Chem. Phys.*, **130**, (2009).
[71] I. Shavitt and L.T. Redmon, *J. Chem. Phys.*, **73**, 5711–5717 (1980).
[72] J. Seino and M. Hada, *Chem. Phys. Lett.*, **461**, 327–331 (2008).
[73] M. Filatov and D. Cremer, *J. Chem. Phys.*, **122**, (2005).
[74] R. Samzow, B.A. Hess, and G. Jansen, **1227**, (2020).
[75] C. Park and J.E. Almlöf, *Chem. Phys. Lett.*, **231**, 269–276 (1994).

Acknowledgement

The author would like to express great appreciation to professor Haruyuki Nakano for his variable discussion, advice, and encouragement. The author would also like to thank Dr. Yhoshihiro Watanabe and Dr, Satoshi Suzuki for helpful comment and discussion. The author thanks to members of Nakano research group. The author thanks to all colabolators; Prof. Norio Yoshida, Dr. Masahiro Higashi, and Dr. Nobuki Inoue for helpfull comment.